Laser Physics, Vol. 2, No. 4, 1992.

Review

Generation-Diffusion-Deformational Instabilities and Formation of Ordered Defect Structures on Surfaces of Solids under the Action of Strong Laser Beams

V. I. Emel'yanov

International Laser Center, Moscow State University, Moscow 119899, Russia

Manuscript received March 7, 1992

Abstract – Theoretical and experimental results, obtained in studies of a broad novel class of laser-induced surface instabilities are presented.

Contents:

1. INTRODUCTION

1.1. General Characteristics of Generation-Diffusion-Deformational Instabilities

One encounters permanent structural and morphological changes in matter interacting with strong laser radiation with energy density $W \lesssim W_m$, where W_m is the threshold energy density of melting, in various fields of laser physics [1] and laser technology. Among them, one can list such phenomena as the gradual and catastrophic degradation of light emitting devices [2], cumulative laser damage of optical components [3], nonuniform melting of the semiconductor surface (Sec. 5.3.2), ultrafast laser induced structural phase transitions on the semiconductor surfaces [4 - 9], and various processes of laser-induced treatment of materials: multipulse laser annealing [10], recrystallization of thin amorphous films [11, 12], thin film deposition [13] and other applications.

The time of light-matter interaction necessary for inducing structural changes in materials responsible for these phenomena can be varied from 10^{-13} s to minutes, depending on the value of W and other conditions of irradiation and the material used.

These changes can be the aim of laser treatment, for example, in the case of laser material treatment, or be undesirable or disallowed in the case of gradual or catastrophic degradation or damage.

Studies of the nature of laser-induced structural changes are not only of scientific interest, but are also of great practical importance because understanding of the physics of the process can enable one to control the latter.

The structural changes induced by a laser beam occur in the lattice subsystem of the material (which in most cases of interest can be considered as an elastic continuum), whereas laser radiation of the wavelength we are interested in excites directly only the electronic subsystem. This excitation creates plasma of nonequilibrium carriers in the subsurface layer of semiconductors, relaxation of this plasma leading to lattice heating. The nonuniform plasma and lattice heating give rise to strong deformation of the subsurface layer of the material.

These three factors of laser action, namely, electronic excitation, heating, and deformation under the conditions of high level of excitation lead to intensive generation of defects, including point defects (electron-hole pairs (i.e., the plasma itself), vacancies and interstitials) and extended defects (voids, dislocation loops, subboundaries and other extended imperfections).[1] Intensive generation of defects takes place on the surface and in the subsurface layer in a variety of laser-treatment processes, carried out in different materials and in different modes of laser irradiation, due to the above-mentioned factors of laser action or other generation mechanisms. We can mention here at least three processes of defect production which occur during the above listed interactions between laser beams and solids, which we shall be concerned with:

– point defect generation in pulsed laser radiation interaction with strongly absorbing semiconductors and metals in modes prior to melting [16];

– capture of high concentrations of vacancies and interstitials in rapid laser-induced melt solidification [17, 18];

– intensive formation of point defects in laser-assisted thin film deposition [19].

The dense fields of defect concentrations are produced also under the irradiation of solids by energetic particle beams [20] and under ion implantation [21].

These point and also extended defects, being rigid inclusions into the elastic continuum, deform the latter [30, 31] and vice versa, the deformation changes the spatiotemporal distribution of the defect field.

Thus from this point of view, a situation universal for all the above listed, and at first sight quite different, phenomena of laser beam-solid interactions arises: the laser treated material can be modelled by two subsystems – the elastic continuum and the field of defect concentration, interacting with each other. In this work we adopt and develop this defect-deformation (DD) model of a solid and apply it to various practical problems mentioned above.

Because of the monotonous transverse distribution of energy in the excitation beam cross-section (for example, the Gaussian distribution in Fig. 1), the concentration of generated defects is usually assumed to decrease monotonously along the surface as the distance from the center of the irradiated spot increases (Fig. 1).

In this work we want to show theoretically and experimentally that both the process of defect generation itself and the generated dense field of defect concentration are unstable with respect to localized or periodically extended perturbations, the resultant instability leading to formation of defect ordered structures of various types. We call this novel broad class of laser-driven surface instabilities "generation-diffusion-deformational instabilities" (GDDI), because they develop due to the interaction of the defect concentration field, generated by laser radiation and changing due to diffusion, with self-consistent deformation of the elastic continuum of a host material. The onset of GDDI is accompanied by abrupt, and in some cases catastrophic changes of the optical, mechanical, and electrophysical properties of the materials, which have various manifestations.

Particular cases are possible when instability development is completed during the process of generation of defects without any participation of diffusion. We call these instabilities "generation-deformational instabilities" (GDI). Instabilities developing due to diffusion when the generation process is over are called "diffusion-deformational instabilities" (DDI).

GDI starts when the intensity of the laser pump I exceeds a particular critical value I_{cr}, while DDI devel-

[1] Although electron-hole pairs are excitations in the electronic spectrum and not lattice imperfections, we include them into the unified treatment here because of the analogy of their behavior in the effects considered below. Note that standard classification of defects also includes electron-hole pairs as one of the types of point defects [14, 15].

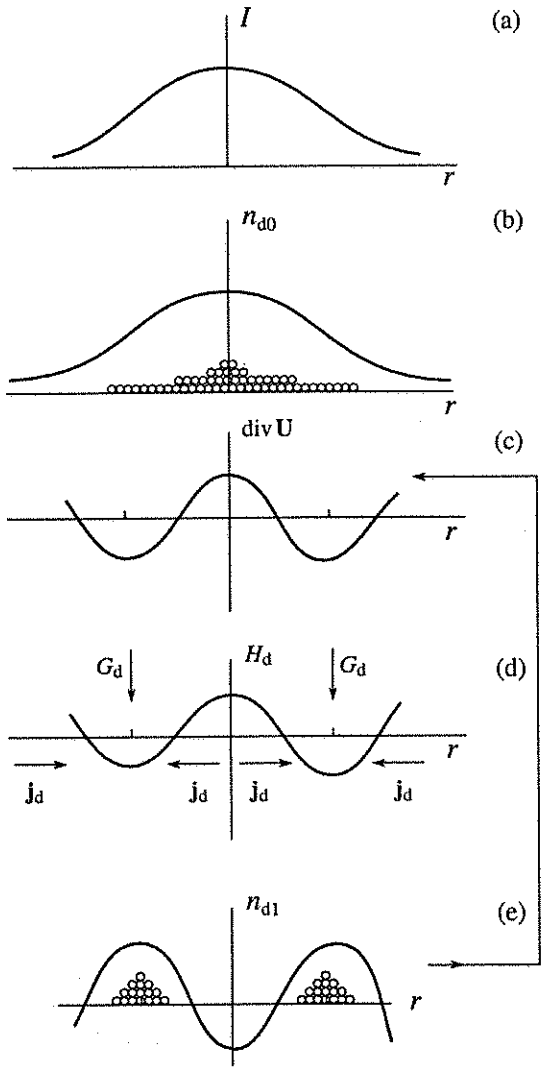

Fig. 1. *Physical mechanism of feedback in point defect GDDI (r is the coordinate along the surface): laser intensity distribution (a); monotonous distribution of laser generated defects (b); fluctuation harmonic of surface strain (c); periodic potential wells due to interaction energy (1.1) (d); j_d are deformation-induced defect fluxes, G_d is deformation-enhanced defect generation rate; Fourier harmonic of defect concentration arising due to j_d and G_d (e). The feedback is due to the force $F_d \sim$ grad n_{d1}.*

ops when the number density of point (or extended) defects n_d exceeds a particular critical value n_{cr} ($n_{cr} \sim 10^{19} - 10^{20}$ cm^{-3}).

Either extended periodic or localized DD structures are created on the surface due to the point defect GDDI. These periodic or quasilocalized point defect clusters are embryonic extended defects and transform to them, forming periodic or quasilocalized void fields or dislocation loop concentrations. In the case where localized extended defects are formed in this way with their number density exceeding a particular value, the second stage of DDI can take place with self-consistent spatial redistribution of extended defects, leading to formation of periodic extended defects-deformational surface structures. Thus, at sufficiently high levels of excitation, GDDI in the long run is ended with formation of periodic extended defects-deformational structures, according to two possible scenarios: (1) accumulation of point defects, threshold formation of periodic point defects-deformational structures, formation of periodic extended defects-deformational structures; or (2) accumulation of point defects, threshold formation of extended defects, threshold formation of periodic extended defects-deformational structures. The formation of these structures leads eventually to material damage. We consider below this hierarchy of transformations of coupled fields of defect concentrations and deformations from the unified point of view of the DD model of the solid.

The development of the concept of GDDI was stimulated by numerous observations of laser-driven formation of surface periodic structures in the form of one and two-dimensional gratings, concentric rings or radial ring structures of different nature (periodic surface relief modulations, alternations of different phases or pileups of voids or dislocations, and so on). The particular geometric forms of these structures are determined by either symmetry of the laser field – in the case of isotropic surface, or by crystalline symmetry of the surface; cases where the symmetry of the structure is determined by the interplay of the above two symmetries also exist. In general, the period of these surface structures is determined by the level of surface excitation. It is not proportional to the wavelength of excitation radiation and is insensitive to its angle of incidence. No spatial coherence of radiation is needed for excitation of these structures. In this review, we present numerous examples of such structures and identify them as the DD structures.

The DD structures differ qualitatively from the periodic surface relief gratings (surface ripples), appearing on surfaces of semiconductors and metals due to interference instabilities occurring under the action of spatially coherent linearly polarized laser light (see Refs. [22 - 26]). The periods of surface ripples are proportional to the wavelength of the excitation radiation, and depend on the angle of incidence, and the wave vector of the surface ripples' grating is collinear with the vector of polarization of the laser wave. Due to this difference it is easy to discriminate surface ripples from the DD structures.

One of the most striking examples of a DD structure is the universal "star"-structure, which is recorded under quite different conditions of irradiation and on quite different materials. Similar "star"-structures were observed, for example, under picosecond laser irradiation of the VO_2 films (Fig. 4), irradiation of metal surfaces with millisecond pulses (Fig. 11), cw-laser irradiation of thin metal plates (Fig. 13) and films (Fig. 14), in laser-induced recrystallization of amorphous semiconductor films (Fig. 38), and in laser etching of semiconductor films [69]. The similarity of geometry of these "star"-structures indicates certain universal mechanism of their formation in quite different materials and under widely varying conditions of laser irradiation. To explain formation of the "star" and

other DD structures we proposed the concept of GDDI [27 - 29]. Since then, a number of experimental and theoretical works have been done, dedicated to studies of the DD structures' formation, and development of the GDDI concept and its application to interpretation of different phenomena, connected with strong laser beam-solid interactions. The present work is the review of the original results, obtained in both theoretical and experimental studies of GDDI.

The physical mechanism of GDDI consists in the following. A strong laser beam generates a large number of point defects in the subsurface layer. In continuum approximation [30], we describe the defect subsystem by the field of defect concentration $n_d(\mathbf{r}, t)$, where the subscript d denotes the particular type of point or extended defects ($d = e$ for electron-hole pairs, $d = v$ for vacancies and so on); $\mathbf{r} = \{x, y, z\}$ is the radius-vector of the space point. The fields of defect concentrations together with the temperature field $T(\mathbf{r}, t)$ comprise the generation-diffusion (GD) subsystem, described by the generalized GD-variable Y_j ($Y_j = n_d$ or T).

The second subsystem is the elastic continuum of the host material, described by the displacement vector $\mathbf{U}(\mathbf{r}, t) = \{U_x, U_y, U_z\}$ with boundary conditions corresponding to a particular case considered (the bulk, the surface of the material or the thin film).

Coupling between the GD and D fields occurs due to the point defect-strain interaction, the energy density of which for an isotropic solid or crystal of cubic symmetry is given by Refs. [30, 31]

$$H_d = -\theta_d n_d \operatorname{div} \mathbf{U}_d , \qquad (1.1)$$

where for vacancies and interstitials $\theta_d = \operatorname{sgn} d K a^3$, K is the bulk elastic modulus, a is the lattice parameter and $\operatorname{sgn} v = -1$, $\operatorname{sgn} i = +1$ [30, 31]. Eq. (1.1) describes also the case of electron-hole-strain interactions, for which θ_d ($d = e$) is the interband deformation potential with $\operatorname{sgn} d$ depending on the type of energy band valley pumped by laser [32]. For dislocation-shear strain interaction the coupling energy is different from Eq. (1.10) (Sec. 7.1).

The adoption of point defect-strain interaction energy in the form of Eq. (1.1) is a crucial step in the development of the GDDI model because it automatically determines the GD-D coupling coefficients both in the equation for the displacement vector and in the effective diffusion equation for defects. In the case of DDI with the thermal fluctuation generation of vacancies and interstitials the anzats (1.1) automatically ensures the positive feedback between the GD and D subsystems, and in the case of GDI for electron-hole pairs the sign of the feedback can be positive or negative depending on the particular case.

The feedback link under the GDDI is as follows. The fluctuation of deformation modulates the energy of formation or of the migration of a defect $E_d = E_d^0 - \theta_d \operatorname{div} \mathbf{U}$ and also modulates the absorption coefficient that gives rise to modulation of defect production rate, diffusion rate and medium heating rate. In the DDI the spatial redistribution of defects occurs due to deformation induced defect fluxes which are found from Eq. (1.1): the force acting on a defect

$$\mathbf{f}_d = -\operatorname{grad} H_d$$

gives rise to the defect flux

$$\mathbf{j}_d = \frac{n_d \theta_d D_d}{kT} \operatorname{grad} \operatorname{div} \mathbf{U}, \qquad (1.2)$$

where D_d is the diffusion coefficient. The resultant appearance of the inhomogeneous GD-fields gives rise to appearance of forces $\mathbf{F}_n \sim \operatorname{grad} n_d$ and $\mathbf{F}_T \sim \operatorname{grad} T$ deforming the elastic continuum and enhancing the seeding deformation fluctuation. Thus there appears positive feedback, leading after exceeding the critical value of the externally controlled parameter, to onset of the GDDI (see Fig. 1).

In the GDDI, certain spatial Fourier components of the coupled GD-deformational fields grow exponentially in time. In the general case they have the following structure

$$\begin{aligned} (\partial U_i / \partial x_j)_{\mathbf{q}} &= A_{ij}(\mathbf{q})\, \Phi(\mathbf{qr}) \exp\{i\omega_q t + i\lambda t - \gamma_q z\}, \\ Y_j &= B_j(\mathbf{q})\, \Phi(\mathbf{qr}) \exp\{i\omega_q t + i\lambda t - \gamma_q z\}, \end{aligned} \qquad (1.3)$$

where the wave vector $\mathbf{q}$ lies in the plane of nondeformed surface $z = 0$ (the z-axis is directed inside the medium), $\lambda = \lambda(\mathbf{q})$ is the growth rate and $\gamma_q > 0$ is the inverse value of surface field penetration depth into the bulk (usually $\gamma_q \sim q$, see Fig. 2).

The eigenfunctions of Laplace operator $\Phi(\mathbf{qr})$ in Eq. (1.3) describe the structure of coupled fields on the surface. Their particular forms are determined by the symmetry of the problem in the surface plane determined by either a crystallographic symmetry, or by a symmetry of the laser field (see Fig. 2).

The cases of excitation of dynamic coupled GDD fields at the surface, where $\omega_q \neq 0$ and $\lambda > 0$, as well as generation of static fields ($\omega_q = 0$, $\lambda > 0$) are possible.

The time of GDDI development t_d (its order of magnitude) is determined by the inverse growth rate $t_d \sim \lambda^{-1}$. GDDI develops under the conditions of the competition of the pump and dissipation due to diffusion and recombination (see Fig. 1), its growth rate in general having the following structure

$$\lambda = -\tau_{d\,\mathrm{eff}}^{-1} - D_d q^2 + G_d(q), \qquad (1.4)$$

where $\tau_{d\,\mathrm{eff}}^{-1}$ is the effective linear and nonlinear recombination constant, and $G(q)$ describes distribution of the pump over the q-modes.

At the GDDI threshold, when pump intensity (dose) is equal to its critical value $G_d(q) = G_{cr}(q)$, one has $\lambda = 0$, and above the threshold the growth rate can be represented in the form

$$\lambda = (\tau_{d\,\mathrm{eff}}^{-1} + D_d q^2)\left(\frac{G_d(q)}{G_d(q)} - 1\right).$$

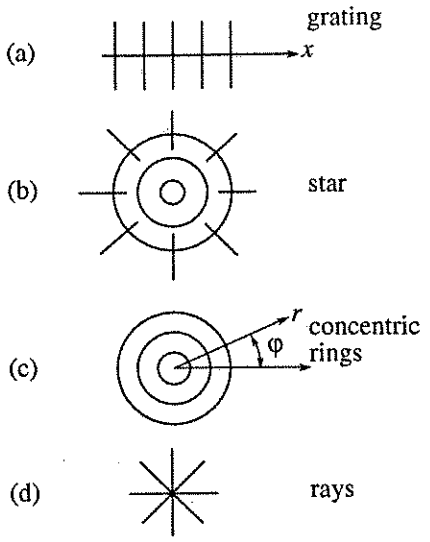

Fig. 2a. *Eigenfunctions of Laplace operator and visual representations of geometry of the corresponding surface GD-D fields exp iqx (a); $J_m(qr)\cos m\varphi$ (b); $J_0(qr)$ (c); $r^m \cos m\varphi$ (d) (see Fig. 2b for comparison).*

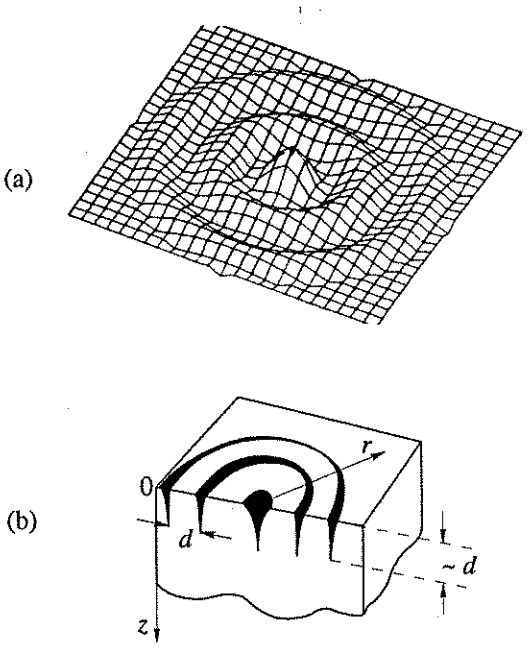

Fig. 2b. *Surface concentric ring DD structure. Computer simulation of m = 0 Bessel function $J_0(qr)$ corresponding to Fig. 2a (a); schematic view of sample cross-section: DD structure penetrates from the surface into the bulk by the distance of the order of structure period (b).*

Thus the dissipation rate determines the order of magnitude of the time of GDDI development:

$$t_d \sim (\tau_{d\,eff}^{-1} + D_d q_{max}^2), \qquad (1.5)$$

where q_{max} is the wave number of interest (for example, that corresponding to the maximum of the dependence $\lambda = \lambda(\mathbf{q})$). Depending on the magnitudes of $\tau_{d\,eff}^{-1}$ and D_d, the value of t_d varies from 10^{-13} - 10^{-11} s (for electron-strain instability) to 10^2 s (for voids and dislocations).

The dependence of the growth rate λ on $\mathbf{q}$ determines whether the resultant GDD field will be localized or periodically extended. In the case where the dependence $\lambda = \lambda(\mathbf{q})$ has a maximum (Fig. 3a), periodic coupled fields are generated. In the case of monotonously decreasing dependence $\lambda = \lambda(\mathbf{q})$ (Fig. 3b), a quasi-localized GDD field is formed, which is a cluster of defects in a self-consistent deformation well (Figs. 1d, 1e).

The competition between the pumping and dissipation, reflected by Eq. (1.4), is a characteristic feature of so called dissipative instabilities, examples of which are readily found in Refs. [33, 34]. The GDDI represent a novel type of dissipative instability closest to the well-known diffusion-diffusion instability described by two coupled diffusion-reaction equations [34 - 36]. In the GDD system one of the diffusion fields is replaced by the field of deformation. This replacement leads to qualitative changes of system behavior, the most dramatic of which is the possibility of creating metastable or stable structures, persisting after the end of the pumping (it is known that the most characteristic feature of usual dissipative instabilities and resultant stationary dissipative structures is the presence of pumping [34 - 36]).

In fact, stabilization of GDDI occurs owing to the nonlinearity of either the elastic continuum or of the diffusion field. In the case of crystal lattice imperfections, generation of static fields leads to creation of defect-deformational metastable (or stable) surface structures, being pileups of defects captured inside the self-consistent deformation wells. The local (or global) minimum of the defect-elastic free energy, corresponding to the appearance of a new spatially nonuniform coupled defect-deformation field, appears at the critical value of the external control parameter corresponding to the onset of GDDI (see Sec. 4.3.4). If the dimension L_d of these pileups of defects (vacancies or interstitials, for example) turns out to be less then the mean distance between the defect sinks l_d, then the defects, captured in self-consistent strain wells cannot recombine, and such a state can exist for a long time (the diffusion is deformationally suppressed).

The review contains the following sections. Sec. 2 describes a prototype of the GDDI – electron-deformation-thermal instability (EDTI) under interband electronic transitions, induced by powerful laser pulses with durations $\tau_p \sim 10^{-9}$ - 10^{-13} s and quantum energy $\hbar\omega > E_g$ the fundamental band gap. EDTI leads to formation of coupled periodic (along the surface) fields of deformation and electron-hole pairs concentration (and temperature, if $\tau_e > \tau_{e\text{-}ph}$ – the time of electron-phonon relaxation) on the surface during the time interval $\tau_e \sim 10^{-9}$ - 10^{-13} s (depending on the laser pump intensity). These fields may be either of dynamic nature (coupled surface acoustic-diffusion waves) or of static nature. It is shown that the periodic deformationally induced modulation of the fundamental band gap may

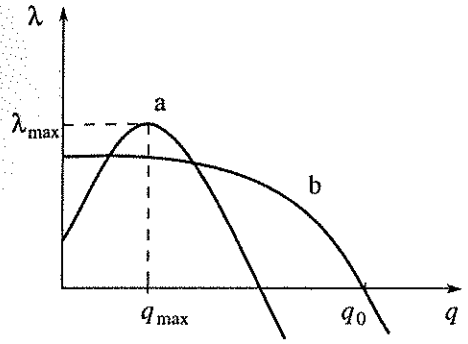

Fig. 3. *The schematic view of typical dependencies of GDDI growth rate λ on the wave number q. Extended periodic DD structure is formed with the period $2\pi / q_{max}$ (a); quasilocalized DD structure is formed with a few oscillations with the period $2\pi / q_0$ (b).*

lead to semiconductor-metal phase transition with the formation of surface periodic superstructures of alternating metal and semiconductor phases. The experimental results on inducing such superstructures in VO_2 films by using picosecond lasers are interpreted from the viewpoint of EDTI. The possibility of ultrafast laser-induced phase transition to a centrosymmetric semiconductor-like phase in GaAs under the action of powerful femtosecond laser pulses is shown and relevant experimental results are discussed.

In Sec. 3 the electron-deformation-thermal model (EDT) of pulsed laser-induced point defect generation in semiconductors under the conditions of interband electronic transitions is developed. The experimental results, obtained for Ge and GaAs are interpreted from the viewpoint of the EDT model. The EDT mechanism of point defect generation in semiconductors is shown to result in formation of surface periodic defect structures under the conditions when the EDTI is developed. The relevant experimental results obtained under nanosecond excimer laser excitation of interband transitions in GaP are presented.

Sec. 4 is devoted to laser-induced point defect (vacancy and interstitial) generation in metals and semiconductors and formation of periodic surface structures of point defects. The theory of vacancy generation-deformational instability on the surface is developed by analogy with the EDTI theory. The experimental results on surface "star"-structure formation under millisecond laser irradiation of the Ti surface are discussed. It is shown that in thin films the bending deformations may play the dominant role in GDI, leading to the specific dependence of the period of the DD structures d on the film thickness h ($d \sim h$). In Sec. 4.3, the diffusion-deformational instability occurring due to the defect spatial redistribution along the surface by diffusion and deformationally-induced defects fluxes is considered. DDI with participation of vacancies and interstitials is considered in Sec. 4.3.2. In Sec. 4.3.4 the DDI theory is extended to the case of electron-hole pairs. It is shown that the DD structures generated due to the DDI are metastable self-consistent states of coupled defect-deformational interaction. The experimental results on surface grating formation, obtained in the case of millisecond laser irradiation of Si surfaces are interpreted from the viewpoint of point defect DDI. It is shown that one can control the direction of deformationally-induced defect fluxes along the surface by means of strong linear-polarized laser radiation. Another interesting possibility following the experimental results obtained is the interaction between the interference surface ripples and defect grating, leading to periodic defect entrainment by the interference surface light field.

As an example of another application of DDI theory, a novel mechanism of subboundary formation in zone-melting recrystallization of a semiconductor on insulator (SOI) films is developed, which explains from a unified point of view the basic experimental results obtained in the studies of the technologically important SOI-problem.

The theory of formation of extended defects due to the threshold development of DDI in a dense point defect field interacting with a strain field is presented in Sec. 5. The DDI theory predicts the threshold formation of localized point defect clusters captured into self-consistent strain wells, where concentration of the point defects exceeds the critical value $n_d \sim 10^{19}$ cm^{-3}, and predicts also the geometric form of these clusters and permits one to evaluate the pressure inside them. Depending on the particular conditions, defect clustering leads to either voids or dislocation loop generation. The expressions for the number of generated loops and their radius are obtained.

As applications of the DDI theory of threshold extended defect generation we consider the mechanism of threshold degradation of injection lasers, yielding the explicit analytical expression for laser lifetime τ as a function of the driving current, which is in good agreement with the empirical law (Sec. 5.3.1). As another application we consider the mechanisms of the nonuniform faceted melting of Si surface by laser radiation (Sec. 5.3.2) and of cumulative explosive laser damage of semiconductors (Sec. 5.3.3).

In Secs. 6 and 7 we consider the situation for which a high density of extended defects is created on the surfaces of solids either due to the DD or some other condensation mechanism, or due to laser induced deformations. Sec. 6 is devoted to consideration of the void-deformational instability in thin films, occurring when the number density of voids exceeds the critical value. The theory explains the experimental results on the formation of periodic concentric ring void structures in laser deposition of thin metal films. In Sec. 7 two types of dislocation-deformational instabilities are considered. The first one occurs due to the dislocation glide and leads to the formation of periodic dislocation pile-ups in the gliding plane (the in-plane structure). The second one, occurring due to the dislocation climbing with the exchange of vacancies, leads to the formation of interplane ordered dislocation structures in the form of periodic ideally straight lines. The experimentally

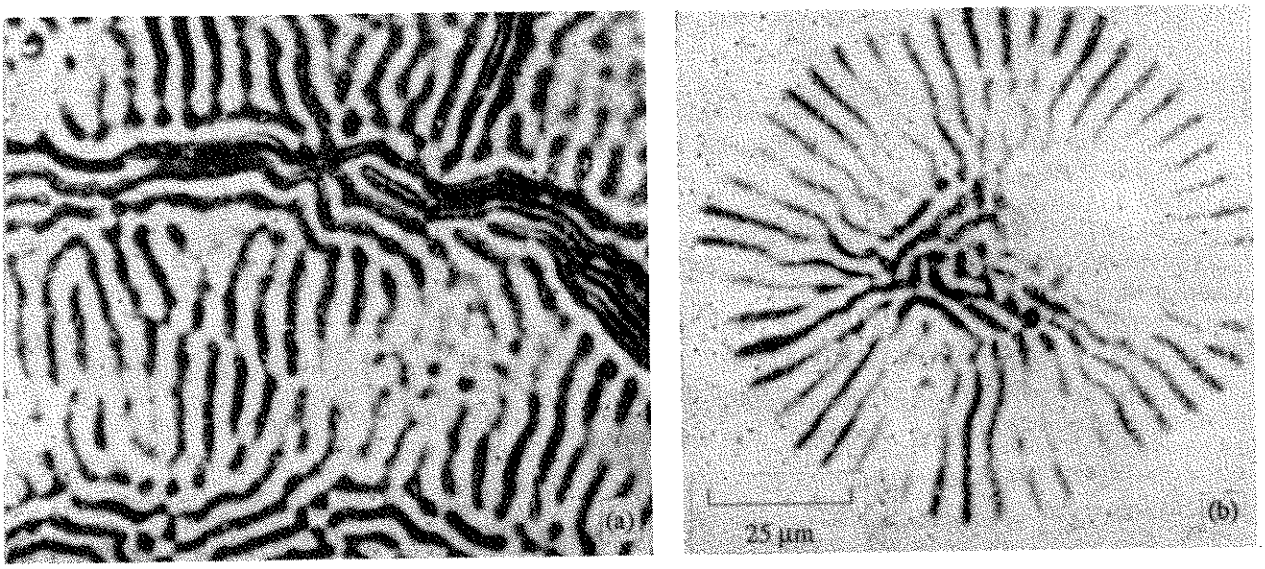

Fig. 4. *Surface periodic metal-semiconductor structure induced in VO_2 film by the picosecond laser pulse [37]. Grating: one-dimensional laser intensity distribution (a); "star"-structure: axial laser intensity distribution (b). The ray multiplication by bifurcation with increase in the distance from the center of the irradiated spot is clearly seen (cf. Fig. 11).*

observed dislocation periodic structures of both types are discussed from the point of view of the theory of dislocational-deformational instabilities.

Sec. 8 is devoted to consideration of exothermal laser-induced instabilities with the participation of deformations. As an example we consider the crystallization-deformation-thermal instability (CDTI) on the surface of amorphous semiconductors and in thin semiconductor films. In these instabilities the laser pulse serves as only an initial activator, and the instability itself develops due to the latent heat of crystallization. It is shown that CDTI leads to formation of the periodic surface structures of different (amorphous and crystalline) phases.

In conclusion, in Sec. 9 we summarize our discussion of GDDI and outline the perspectives of future research in this field of laser physics.

2. ELECTRON-DEFORMATION-THERMAL INSTABILITY (EDTI) UNDER INTERBAND TRANSITIONS IN SEMICONDUCTORS

2.1. Introduction

In this section we consider the prototype of GDDI – the electron-deformation-thermal instability developing under the action of short (10^{-8} - 10^{-13} s) laser pulses on strongly absorbing (in the range of interband absorption) semiconductors. The defects of interest are the electron-hole pairs. Here we consider the case of GDI (the case of electron-hole DDI is considered in Sec. 4.3.4). The development of electron GDDI in semiconductors is shown to lead to ultrafast phase transitions in semiconductors.

The physics of ultrafast laser-induced surface phase transitions is interesting for applied problems of pulsed-laser modification of surface layers of semiconductors, which are currently attracting much attention. Phase transitions induced by laser pulses are due to the change in the state of the lattice subsystem, whereas laser radiation with the photon energy $\hbar\omega > E_g$ (where E_g is the width of the band gap) interacts with the electron subsystem. Thus, the electron-phonon interaction and the corresponding transformation of the absorbed energy play a key role in the effects mentioned above.

The usual mechanism by which the absorbed energy is transferred to the lattice consists of electron-electron, electron-phonon, and phonon-phonon relaxation stages with relaxation times τ_{rel} of the order of a picosecond. The resultant spatial distribution of the lattice changes should reflect a monotonic reduction of the radiation intensity away from the center of a laser-illuminated spot and an exponential reduction of the absorbed energy with depth in the investigated medium (with a characteristic scale at least equal to the linear absorption length γ_0^{-1}).

However, a number of experimental results obtained using high-power ultrashort laser pulses cannot be explained on the basis of these standard representations. Thus, instead of a monotonic pattern, it is frequently found that ordered surface structures are formed. For example, irradiation with picosecond laser pulses of a semiconducting phase of VO_2 creates a spatially periodic surface pattern representing an alternation of metallic and insulating phases, and if the laser field has axial symmetry, it is found that concentric rings appear at the center of the spot and radial rays are formed at the periphery (a "star" pattern is observed), whereas when the field has slab geometry it is found that one-dimensional gratings are obtained (Fig. 4) [37]. Pulsed laser irradiation of the surface of a semiconductor also gives rise to concentric ring structures representing an alter-

nation of crystalline and amorphous phases [38]. Some results support a nonlinear mechanism of transfer of the laser energy to the lattice at high pump intensities. For example, a reduction in the absorption length by an order of magnitude compared with γ_0^{-1} is reported in Ref. [39]. It was experimentally shown in Refs. [6 - 9] that high-power femtosecond pulses induce structural changes (or superfast transition to a new state (see Sec. 2.7)) of the crystalline lattice in the subsurface layer of a semiconductor during a pulse, i.e., in a time much shorter than τ_{rel}.

These experimental observations can be interpreted in terms of the formation of laser-induced instabilities on the surface of a semiconductor, leading to a periodic change in the resultant state of the lattice along the semiconductor surface and a strong increase in the effective optical absorption coefficient.

We shall review in this section two new laser-induced instabilities on the surface of a semiconductor: an electron-deformation instability (EDI) and a deformation-thermal instability (DTI), the theory of which can account for the experimental results (in particular the formation of the ordered structures) mentioned above. These two instabilities can occur simultaneously, giving rise to an electron-deformation-thermal instability (EDTI) [27, 41, 42].

The physical mechanism of the EDTI is as follows. The surface deformation $\xi = \mathrm{div}\,\mathbf{U}$ ($\mathbf{U}$ is the displacement vector of the medium), electron-hole plasma with concentration n_e and temperature T modulate spatially the width of the band gap:

$$E_g = E_{g0} - \theta\xi - \beta_n n_e - \beta_T T, \qquad (2.1)$$

where E_{g0} is the equilibrium value of the band gap: $dE_g / d\xi = \theta$; $\theta = \theta_{cc} - \theta_{vv}$; θ_{cc} and θ_{vv} are the deformation potentials of the conduction and valence bands, respectively. The phenomenologically introduced coefficient $\beta_n = |\partial E_g / \partial n_e| > 0$ describes the reduction in E_g because of the breaking of covalent bonds when electrons are transferred from bonding states in the valence band to antibonding states in the conduction band [43], while the coefficient $\beta_T = |\partial E_g / \partial T| > 0$ allows for the reduction in E_g as a result of heating [44]. Modulation of E_g results in modulation of the interband optical absorption coefficient, causing accordingly an additional modulation of n_e and E_g. The resultant forces $\mathbf{F}_n = -\theta\,\mathrm{grad}\,n_e$ and $\mathbf{F}_T = -K\alpha\,\mathrm{grad}\,T$ (K is the bulk modulus and α is the thermal expansion coefficient) maintain initial displacements of the lattice, giving rise to an instability of the amplitude of the surface strain ξ and also of the carrier density n_e and the temperature T when a certain critical intensity of the laser pump radiation is exceeded.

In this section we consider the solution of the boundary value problem of the development of the EDTI on the surface of a semiconductor under strong optical absorption conditions. A general dispersion equation is obtained for the EDTI and its solution determines the rate of the exponential growth (with time) of the Fourier amplitudes of the coupled fields of ξ, n_e, and T on the wave vector ($\lambda = \lambda(\mathbf{q}) = \lambda' + i\lambda''$). It follows from this equation that three qualitatively different instabilities can appear under the EDTI conditions. The first is the instability of surface acoustic waves ($\lambda'' \neq 0$, $\lambda' > 0$), which is initiated by thermal surface acoustic waves. The second is an instability (softening) of the acoustic surface wave frequencies. The third is the instability of surface static deformations ($\lambda'' = 0$, $\lambda' > 0$). In the last case the instability begins from the initial fluctuations of the temperature or carrier density. The present section represents a detailed study of the last instability.

We shall show that the EDTI can create complex ordered configurations of the coupled surface fields of ξ, n_e, and T (in the form of gratings, rings, rays, "stars," and radial-ring cells formed by the intersection of rings and rays, Fig. 2). The periods of these structures are expressed as a function of the parameters of the investigated material and of the intensity and duration of the laser pulses, and determine how far these structures penetrate from the surface into the material. A nonlinear steady-state EDTI regime is considered, which becomes stabilized because of the nonlinear Auger recombination of carriers and also because of the optoacoustic nonlinearity. The steady-state values of the Fourier amplitudes of strain, carrier density, and temperature are determined as a function of the wave vector $\mathbf{q}$ and of the pump radiation intensity. It is shown that the modulation amplitude of the band gap width along the surface, in accordance with the mechanism described by Eq. (2.1), may in principle reach values at which E_g vanishes in a spatially periodic manner, i.e., a laser induced semiconductor-metal transition accompanied by the formation of ordered surface structures is induced.

The present paper's allowance for the deformations (strains) and for the influence of the surface is a fundamentally novel feature of the theory of laser-induced insulator-metal phase transition, which can explain the formation of complex periodic structures on the surface (in earlier works [39, 40] laser-induced semiconductor-metal phase transition was investigated without allowance for these two factors). Numerical estimates of the parameters of these structures showed that the EDTI mechanism may be responsible for their formation.

2.2. Closed System of Equations of EDTI

We shall consider a two-band semiconductor filling the semispace $z > 0$ and assume that a laser wave is incident normally on the $z = 0$ surface:

$$\mathbf{E}(\mathbf{r}, t) = \mathbf{E}\exp(-i\omega t + ikz) + \mathrm{c.c.} \qquad (2.2)$$

Here $\mathbf{E} = \mathbf{E}(\mathbf{r})f(t)$; $f(t) = 1$, when $0 \le t \le \tau_p$; $f(t) = 0$, when $t < 0$, $t > \tau_p$; τ_p is the duration of a laser pulse, and $\mathbf{r} = \{x, y\}$.

In the case under discussion ($\varepsilon' \gg 1$, $\varepsilon' \gg \varepsilon''$), the equation for the temperature of the medium is (see Ref. [39])

$$\frac{\partial T}{\partial t} - \chi \Delta T = \frac{2\omega\varepsilon''}{\pi c_v \varepsilon'} |\mathbf{E}|^2 \exp(-\gamma z), \quad (2.3a)$$

where χ is the thermal diffusivity, c_v is the specific heat per unit volume, ε' is the real part of the dielectric permittivity of the medium, $\gamma = \omega\varepsilon'' / c(\varepsilon')^{1/2}$ is the optical absorption coefficient, and c is the velocity of light in a vacuum.

The equation for the density of nonequilibrium carries can be written in the form

$$\frac{\partial n_e}{\partial t} - D_e \Delta n_e + \frac{n_e}{\tau_e} + \gamma_A n_e^3 = \frac{2\varepsilon''}{\pi\hbar\varepsilon'} |\mathbf{E}|^2 \exp(-\gamma z), \quad (2.3b)$$

where D_e is the carrier diffusion coefficient, τ_e is the linear recombination time, and γ_A is the nonlinear Auger recombination constant.

The equation for the displacement vector of the medium with the forces, following from Eq. (1.1) has the form

$$\frac{\partial^2 \mathbf{U}}{\partial t^2} = c_t^2 \Delta \mathbf{U} + (c_l^2 - c_t^2) \operatorname{grad} \operatorname{div} \mathbf{U} + \sum_{j=n,T} f_j \operatorname{grad} Y_j, \quad (2.4)$$

where c_l and c_t are the longitudinal and transverse velocities of sound, $f_n = -\theta / \rho$, $f_T = -K\alpha / \rho$, and ρ is the density of the medium. It follows from Eq. (2.1) that the optical constants ε'' and ε' depend on n_e, T, and ξ. In the range of values of n_e, T, and ξ of interest to us, the dependence of ε'' can be represented in the following form if we use the expression for the interband permittivity of a semiconductor $\varepsilon = \varepsilon' + i\varepsilon'$ and allow for Eq. (2.1):

$$\varepsilon'' = \varepsilon_0'' + \frac{\partial \varepsilon''}{\partial \omega} \frac{1}{\hbar} (\beta_n n_e + \beta_T T + \theta\xi) = \varepsilon_0'' + \varepsilon_1''. \quad (2.5)$$

A similar dependence can be written down also for ε'. However, since in the range of frequencies we are interested in we have $\varepsilon' \gg \varepsilon''$ ($\varepsilon' \sim 10$, $\varepsilon_0'' \sim 10^{-1}$) and $\partial\varepsilon' / \partial\omega \sim \partial\varepsilon'' / \partial\omega$, we shall ignore the change in $\varepsilon' = \text{const}$. Therefore, we have $\gamma = \gamma_0 + \gamma_1$, where $\gamma_1 \propto \varepsilon_1''$.

We can see from Eqs. (2.3) that, in the presence of a laser field, Eq. (2.5) should establish a relationship between the diffusing fields of n_e and T and the deformation (strain) of the medium.

Solutions are developed in the form

$$n_e = n_0 + n_1, \quad T = T_0 + T_1, \quad \xi = \xi_0 + \xi_1,$$
$$\mathbf{U} = \mathbf{U}_0 + \mathbf{U}_1,$$

where n_0, T_0, ξ_0, and $\mathbf{U}_0$ are the solutions of Eqs. (2.3) and (2.4) subject to Eq. (2.5), obtained in the zero-order approximation with respect to n_e, T, and ξ under the appropriate boundary conditions at $z = 0$ (see below). The actual form of these solutions is unimportant for the purpose of the present treatment; the only significant factor is that these solutions are constant along the surface over distances $r \ll r_0$ of interest to us (r_0 is the radius of the laser beam) and vary sufficiently slowly in time over intervals on the order of the instability development time (see below). We shall now consider the stability of the solutions, n_0, T_0, and ξ_0. Linearizing Eqs. (2.3) and applying Eq. (2.5) yields equations for $n_1 \equiv Y_{n1}$ and $T_1 \equiv Y_T$, which can be written in a unified manner

$$\frac{\partial Y_{j1}}{\partial t} + \Delta_j(t) Y_{j1} = (\varepsilon_{j\xi}\xi_1 + \varepsilon_{jT}T_1 + \varepsilon_{jn}n_1) \exp(-\gamma_0 z), \quad (2.6)$$

where $j = n, T$; $\Delta_j(t) = -\chi_j \Delta + \tau_j^{-1}(t)$; $\chi_T = \chi$; $\chi_n = D_e$; $\tau_T^{-1} = 0$, $\tau_n^{-1} = \tau^{-1} + \gamma_A n_0^2(t)$. The coupling coefficients are described by the following expressions

$$\varepsilon_{ji} = 2\frac{\partial \varepsilon''}{\partial \omega} |\mathbf{E}|^2 \sigma_{ji} / \varepsilon' \pi\hbar, \quad i = n, T, \xi,$$
$$\sigma_{n\xi} = \frac{\theta}{\hbar}, \quad \sigma_{nT} = \frac{\beta_T}{\hbar}, \quad \sigma_{nn} = \frac{\beta_n}{\hbar}, \quad (2.6a)$$
$$\sigma_{T\xi} = \frac{\omega\theta}{c_v}, \quad \sigma_{TT} = \frac{\omega\beta_T}{c_v}, \quad \sigma_{Tn} = \frac{\omega\beta_n}{c_v}.$$

The boundary conditions for Y_{ji} can be written in the form

$$\left.\frac{\partial Y_{j1}}{\partial z}\right|_{z=0} = 0, \quad Y_{j1}|_{z=\infty} = 0. \quad (2.7)$$

It should be noted that, in general, the boundary condition at $z = 0$ on a surface with relief is of the form

$$\left.\frac{\partial Y_{ji}}{\partial z}\right|_{z=0} + \left.\frac{\partial^2 Y_{j0}}{\partial z^2}\right|_{z=0} U_{1z}(0) = 0,$$

where $U_{1z}(0)$ is the displacement of the surface points $z = 0$ along z, which describes the surface relief. However, under the conditions of interest to us the additional term is small (its value amounting to 10^{-1} - 10^{-4} of that of the first term, see Sec. 2.6), so that we shall ignore it and use the boundary conditions specified by Eq. (2.7). The nature of the boundary conditions for $\mathbf{U}_1$ depends on the symmetry of the laser field and on the required type of solution (see Sec. 2.3).

The system of Eqs. (2.4) (where $\mathbf{U} = \mathbf{U}_1$, $Y_j = Y_{j1}$) and (2.6) can be solved analytically in two limiting cases: (1) weak optical absorption (bulk case); (2) strong optical absorption when γ_0^{-1} is less than the depths of penetration of the surface material excitations, n_1, T_1, ξ_1 into the medium (surface case). We shall consider the case (2) because it is of greater practical interest. We can then write Eq. (2.6) in a simpler form:

$$\frac{\partial Y_{j1}}{\partial t} + \Delta_{j0}(t) Y_{j1} = (\varepsilon_{j\xi}\xi_1 + \varepsilon_{jT}T_1 + \varepsilon_{jn}n_1)|_{z=0} \exp(-\gamma_0 z). \quad (2.8)$$

Here, $\Delta_{n0} = -D_e\Delta + \tau_{n0}^{-1}$, $\tau_{n0}^{-1} = \tau^{-1} + \gamma_A n_0^2(t)|_{z=0}$, $\Delta_{T0} = -\chi\Delta$.

2.3. General Dispersion Equation for EDTI. Formation of One-Dimensional Surface Gratings

We assume that as result of breakdown of the symmetry of the field or medium, there is some preferred direction x on the $\{x, y\}$ surface. Then, the boundary conditions on the $z = 0$ surface for the vector $\mathbf{U}_l$ can be written in the form (we write $\mathbf{U}_l \equiv \mathbf{U}$)

$$\frac{\partial U_x}{\partial z} + \frac{\partial U_z}{\partial x} = 0, \quad \sum_{j=n,T} \frac{f_j Y_{jl}}{c_l^2} + \frac{\partial U_z}{\partial z} + (1-2\beta)\frac{\partial U_x}{\partial x} = 0, \tag{2.9}$$

where $\beta = c_t^2/c_l^2$. We look for the simultaneous solution of the system of Eqs. (2.4 - 2.6) assuming $\mathbf{E}(\mathbf{r}) = \text{const}$ in Eq. (2.2).

We specify the strain ξ_l and the diffusion field Y_{jl} at $z = 0$:

$$\xi_l = A(t)\exp\left(iqx + \int_0^t \lambda dt\right), \qquad Y_{jl} = A_j(t)\exp\left(iqx + \int_0^t \lambda dt\right), \tag{2.10}$$

where $A(t) = A(q, t)$ is a function proportional to the amplitude of the initial strain and $A_j(t)$ is a slow function of time. This solution describes the surface field of the strain, carrier density, and temperature in the form of one-dimensional gratings (Fig. 2). The solution of Eq. (2.8) satisfying Eq. (2.10) can be found in the form:

$$Y_{jl} = [B_j(t)\exp(-\gamma_0 z) + C_j(t)\exp(-\delta_j z)] \times \exp\left(iqx + \int_0^t \lambda d\right). \tag{2.11}$$

Substituting Eq. (2.11) into Eq. (2.8), allowing for the boundary conditions of Eq. (2.7) and Eqs. (2.10), (2.11), we find that if $\gamma_0 \gg \delta_j$ (i.e., if $C_j \gg B_j$), then

$$Y_{jl} = A\varepsilon_{j\xi}\exp\left(iqx + \int_0^t \lambda dt - \delta_j z\right) \times \left[\chi_j\gamma_0\delta_j\left(1 - \sum_{j=n,T}\frac{\varepsilon_{jj}}{\chi_j\gamma_0\delta_j}\right)\right]^{-1}, \tag{2.12}$$

where

$$\delta_j = \delta_j(t) = \left[q^2 + \frac{\lambda + \tau_{j0}^{-1}(t)}{\chi_j}\right]^{1/2}. \tag{2.13}$$

The functions $f(t) = A_j(t)$, $\delta_j(t)$, $\lambda(t)$ obey the condition for slow change with time $f^{-1}(t)\partial f(t)/\partial t \ll \lambda$, which reduces to the condition that the functions n_0, T_0, and ξ_0 vary little on a scale of λ^{-1} (adiabatic approximation). We now solve Eqs. (2.4) and (2.9). We represent the vector $\mathbf{U}$ in the form $\mathbf{U} = \mathbf{U}_l + \mathbf{U}_t$, where

$$\text{div}\,\mathbf{U}_t = 0, \quad \text{rot}\,\mathbf{U}_l = 0. \tag{2.14}$$

Eq. (2.4) then yields equations for the vectors $\mathbf{U}_t$ and $\mathbf{U}_l$:

$$\frac{\partial^2 \mathbf{U}_\alpha}{\partial t^2} = c_\alpha^2\Delta\mathbf{U}_\alpha + \delta_{\alpha,l}\,\text{grad}\sum_{j=n,T} f_j Y_{jl}, \tag{2.15}$$

where $\alpha = l, t$; $\delta_{\alpha,l} = 1$, if $\alpha = l$; $\delta_{\alpha,l} = 0$, if $\alpha = t$; Y_{jl} is given by Eq. (2.12). The solution of Eq. (2.15) is developed in the form

$$\mathbf{U}_\alpha = \mathbf{B}_\alpha\exp(-k_\alpha z) + \delta_{\alpha,l}\sum_{j=n,T}\mathbf{D}_j\exp(-\delta_j z) \times \exp\left(iqx + \int_0^t \lambda dt\right). \tag{2.16}$$

Substituting Eq. (2.16) into Eq. (2.15) and allowing for the condition (2.14), we express the components B_{lx} and B_{lz} in terms of some constant M, and the components B_{tx} and B_{tz} in terms of a constant N. Then, using the conditions for self-consistency of the solutions described by Eq. (2.16) and of the expression for $\xi_l|_{z=0}$ given by Eq. (2.10), we can express A in terms of M:

$$A = \frac{\lambda^2 M}{c_l^2\Phi},$$

$$\Phi = 1 - \sum_{j=n,T}\frac{R_j c_l^2(q^2 - \delta_j^2)}{\chi_j\gamma_0\delta_j[\lambda^2 + c_l^2(q^2 - \delta_j^2)]} \times \left[1 - \sum_{j=n,T}\frac{\varepsilon_{jj}}{\chi_j\gamma_0\delta_j}\right]^{-1}, \tag{2.17}$$

$$R_n = \frac{2\theta^2}{\varepsilon'\pi\hbar^2\rho c_l^2}\frac{\partial\varepsilon''}{\partial\omega}|E|^2,$$

$$R_T = \frac{2K\alpha\theta\omega}{\varepsilon'\pi\hbar\rho c_v c_l^2}\frac{\partial\varepsilon''}{\partial\omega}|E|^2.$$

The solution with the vector $\mathbf{U}$ can be expressed in terms of M and N, and is of the form

$$U_x = [\kappa_t N\exp(-\kappa_t z) + iqM\exp(-\kappa_l z) - \lambda^2 Miq \times \sum_{j=n,T}\frac{\Phi_j}{\delta_j}\exp(-\delta_j z)\,]\exp\left(iqx + \int_0^t \lambda dt\right). \tag{2.18}$$

$$U_z = (iqN\exp(-\kappa_t z) - \kappa_l M\exp(-\kappa_l z)) + \lambda^2 M \sum_{j=n,T} \Phi_j \exp(-\delta_j z) \exp\left(iqx + \int_0^t \lambda dt\right).$$

Here,

$$\kappa_{l,t} = \left(q^2 + \frac{\lambda^2}{c_{l,t}^2}\right)^{1/2}, \quad (2.19)$$

$$\Phi_j = R_j \{\chi_j \gamma_0 [\lambda^2 + c_l^2 (q^2 - \delta_j^2)]\}^{-1} \times \left[1 - \sum_{j=n,T} \left\{ \frac{\varepsilon_{jj}}{\chi_j \gamma_0 \delta_j} - \frac{R_j c_l^2 (q^2 - \delta_j^2)}{\chi_j \gamma_0 \delta_j [\lambda^2 + c_l^2 (q^2 - \delta_j^2)]} \right\}\right]^{-1} \quad (2.20)$$

Substituting Eq. (2.18) into Eq. (2.9), we obtain two homogeneous equations for M and N:

$$N(\kappa_t^2 + q^2) + 2iqM\left(\kappa_l - \lambda^2 \sum_{j=n,T} \Phi_j\right) = 0,$$
$$-2i\kappa_t qN + (\kappa_t^2 + q^2) M\left(1 - \lambda^2 \sum_{j=n,T} \frac{\Phi_j}{\delta_j}\right) = 0. \quad (2.21)$$

Equating the determinant of the system (2.21) to zero, we obtain a general dispersion equation for the EDTI (which is valid also in the case of radial-ring structures, see Sec. 2.5):

$$4q^2 \kappa_t \kappa_l - (\kappa_t^2 + q^2)^2 = \frac{\lambda^2}{c_l^2} \sum_{j=n,T} R_j \times \left[4q^2 \kappa_t \delta_j - (\kappa_t^2 + q^2)^2\right] / \{\chi_j \gamma_0 \delta_j (\lambda^2 / c_l^2 + q^2 - \delta_j^2) - \sum_{j=n,T} [\varepsilon_{jj} \lambda^2 / c_l^2 + (R_j + \varepsilon_{jj})(q^2 - \delta_j^2)]\}. \quad (2.22)$$

A similar dispersion equation takes place also for the vacancy GDI (see Sec. 4.1).

The dispersion equation (2.22) describes three qualitatively different types of the EDTI. We shall consider each of them separately and limit our treatment of Eq. (2.22) either to an allowance for the EDI for $R_n / D_e \delta_n \gg R_T / \chi \delta_T$ or to the DTI in the opposite limit.

2.3.1. Generation of Surface Acoustic Waves $\lambda = \lambda' + i\lambda''$, $\lambda' > 0$, $\lambda'' \gg \lambda'$

The dispersion equation (2.22) was derived ignoring the viscosity of the medium. If we allow for the viscosity in Eq. (2.22) and also in the corresponding expressions for Φ_j, $\kappa_{l,t}$ and R_j, we have to replace $c_{l,t}^2$ with $c_{l,t}^2 (1 + \eta_{l,t} \lambda / \rho c_{l,t}^2)$, where $\eta_t = \eta$ and $\eta_l = 4\eta/3 + \xi$ (η and ξ are the first and second viscosities). Then, separating the real and imaginary parts in Eq. (2.22) subject to the conditions $\lambda \tau_{j0}^{-1} / \chi_j \ll \lambda''^2 / c_{t,l}^2 q^2$, $2\lambda' \chi_j / c_t^2 \ll 1$, R_j, $\varepsilon_{jj} \ll \chi_j q \gamma_0$, and $\lambda''^2 \eta \chi_j / \rho c_t^4 \ll 1$, we obtain the usual expression for the frequency of the surface acoustic waves: $\lambda'' = \sigma c_t q$; $0.87 < \sigma < 0.95$ [41]. Using the imaginary part of Eq. (2.22) and applying the conditions $\lambda'' / 2D_e q^2 \ll 1$, we obtain the following expression for the growth rate of surface acoustic waves in the EDI case:

$$\lambda' = -\frac{q^2 \sigma^3 \eta}{2\rho} - \frac{4(1 - \sigma^2) c_l^2}{D_e^2 q \sigma^2 \gamma_0} R_n. \quad (2.23)$$

The expression for the growth rate of a surface acoustic wave in the DTI case is found to satisfy the condition $\lambda'' / 2\chi q^2 \gg 1$:

$$\lambda' = -\frac{\sigma q \eta}{2\rho} + \frac{2q(1 - \sigma^2)^{1/2}}{\gamma_0} R_T. \quad (2.24)$$

It is clear from Eqs. (2.17), (2.23), and (2.24) that the generation of surface acoustic waves ($\lambda' > 0$) due to the EDI is possible only if $\partial\varepsilon'' / \partial\omega < 0$, whereas in the case of the DTI, surface acoustic waves can be excited if $\theta \partial\varepsilon'' / \partial\omega > 0$. The critical value of the pump radiation is obtained from Eqs. (2.23) and (2.24) with the condition $\lambda' = 0$.

Eqs. (2.23) and (2.24) were derived ignoring the term in the sum in the denominator of the right-hand side of Eq. (2.22) on the assumption that ε_{jj}, $R_j \ll \chi_j q \gamma_0$. It therefore follows that changes in the band gap due to heating (ε_{TT}) and breaking of covalent bonds (ε_{nn}) are unimportant in the process of excitation of surface acoustic waves (but they may be significant in the generation of static structures (see below)). For more detailed consideration of surface acoustic-diffusion waves and interpretation of experimental results of Ref. [158] on laser-inducted excitation of surface acoustic waves in GaAs, see in Ref. [159].

2.3.2. Softening of Acoustic Frequencies ($\lambda' < 0$, $\lambda'' \to 0$)

Separating Eq. (2.22) into real and imaginary parts satisfying the conditions λ', $\lambda'' \ll q c_{t,l}$, $\lambda' / c_{t,l}$, $\lambda'' / c_{t,l} \ll q$, $[(\lambda' + \tau_{j0}^{-1}) / \chi_j]^{1/2}$, λ', $\lambda'' \ll q^2 \chi_j$, we find that the pump renormalized acoustic frequencies are described by the expression

$$\lambda''^2 = \Omega_q^2 \left(1 - \frac{2\beta}{1 - \beta (q + (q^2 + \tau_{j0}^{-1} / \chi_j)^{1/2})} \times \frac{q R_j}{(q^2 + \tau_{j0}^{-1} / \chi_j)^{1/2} - R_j - \varepsilon_{jj}}\right), \quad (2.25)$$
$$\Omega_q = 2(1 - \beta)^{1/2} q c_t / (3 - 2\beta)^{1/2}.$$

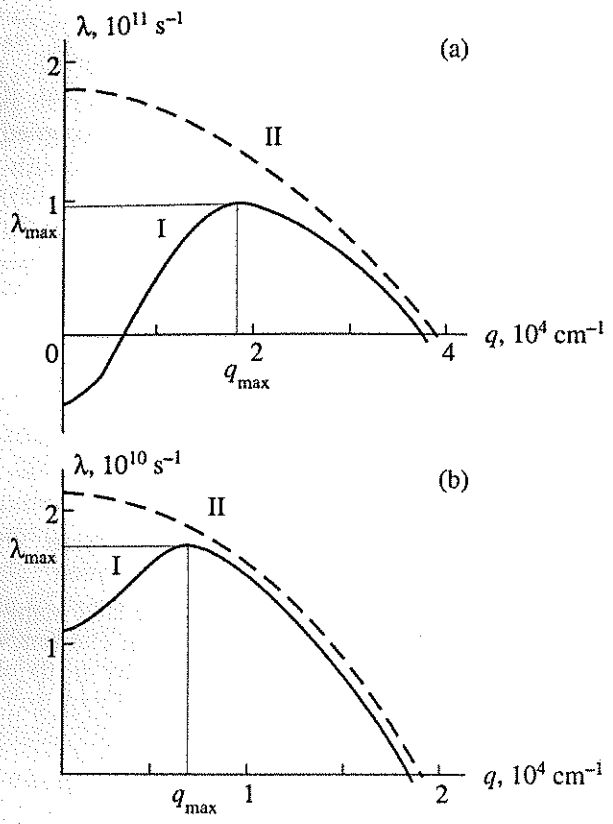

Fig. 5. *Dependence of the EDTI growth rate λ on the wave number q, according to Eq. (2.27). The values of the parameters are given in Sec. 2.6. EDI (a); DTI (b). The curve I corresponds to the case $R_j \gg \varepsilon_{jj}$, II – $R_j \ll \varepsilon_{jj}$ (schematically).*

We can see from Eqs. (2.25) and (2.17) that softening of the acoustic frequencies occurs in the EDI case if $\partial\varepsilon'' / \partial\omega > 0$, whereas in the DTI case it occurs if $\theta\partial\varepsilon'' / \partial\omega > 0$. The critical intensity is found from the condition $\lambda'' = 0$. In fact, the acoustic frequencies do not tend to zero but to $\lambda'' \sim \sigma^2 q^2 \eta / 2\rho \ll \Omega_q$.

2.3.3. Generation of Static Periodic Surface Structures

Substituting $\lambda'' = 0$ in Eq. (2.22) and using the notation $\lambda' \equiv \lambda$, we find the following equation satisfying the conditions $\lambda^2 / c_{t,l}^2 < q^2$, $(\lambda' + \tau_{j0}^{-1}) / \chi_j$

$$(q + \delta_j)\,(\delta_j - q_{R\varepsilon}) = \frac{2\beta}{1-\beta} q_R q, \qquad (2.26)$$

where $q_R = R_j / \chi_j \gamma_0$, $q_{R\varepsilon} = (R_j + \varepsilon_{jj}) / \chi_j \gamma_0$. The solution of Eq. (2.26) is

$$\lambda = \chi_j \left\{ \left[\frac{(q+q_{R\varepsilon})^2}{4} + q q_R \frac{2\beta}{1-\beta} \right]^{1/2} + \frac{q_{R\varepsilon} - q}{2} \right\}^2 - \chi_j q^2 - \tau_{j0}^{-1}. \qquad (2.27)$$

The growth rate reaches its maximum value λ_{max} at point q_{max}, where

$$q_{max} = q_{R\varepsilon} \left[(5a^2 + 6a + 1)^{1/2} - (2a+1) \right], \quad a = \frac{2\beta}{1-\beta} \frac{q_R}{q_{R\varepsilon}}, \qquad (2.28a)$$

$$\lambda_{max} = \chi_j q_{R\varepsilon}^2 \frac{1}{2} \left[(5a+1)\,(5a^2+6a+1)^{1/2} - 11a^2 - 8a + 1 \right]. \qquad (2.28b)$$

The dependence of λ on q according to Eq. (2.27) is plotted for the EDI case in Fig. 5a and for the DTI case in Fig. 5b. If $R_j \gg \varepsilon_{jj}$ (deformation limit of the EDTI), the maximum of $\lambda(\mathbf{q})$ selects a dominant structure with $q = q_{max} \neq 0$, whereas for $R_j \ll \varepsilon_{jj}$ (diffusion limit of the EDTI) the maximum in the spectrum of $\lambda = \lambda(\mathbf{q})$ is reached at $q = 0$. However, even in the diffusion limit of the EDTI a dominant structure with $q \neq 0$ is selected. We can demonstrate this by considering first in greater detail the nature of the initial fluctuation in the EDTI case. At time $t = 0$ the boundary condition of Eq. (2.9) contains $Y_{n1}(t=0) = n_1(t=0)$ and $Y_{T1}(t=0) = T_1(t=0)$, which are the Fourier amplitudes of the initial fluctuations of the population and temperature on the surface (when the simultaneous correlation function is $\langle Y_{j1}(t=0)\, Y_{j1}(t=0)\rangle = \text{const}$ and is independent of q). Using Eq. (2.18) and the relationship $N = -2iq\kappa_1 M / (\kappa_1^2 + q^2)$, which follows from Eq. (2.21), on the assumption that R_j, $\varepsilon_{jj} = 0$ at $t = 0$, and also taking from Eq. (2.27) the expression $\lambda = \lambda(t=0) = -\chi_j q^2 - \tau_{j0}^{-1}$ we obtain from Eq. (2.9)

$$M = -f_j Y_{j1}(t=0) / (1-\beta)\,(\chi_j q^2 + \tau_{j0}^{-1})^2. \qquad (2.29)$$

Eqs. (2.18) and (2.29), together with the relationship between M and N, give the final solution for the vector $\mathbf{U}$ in the EDTI case when static structures are formed. Then, in the diffusion limit ($\varepsilon_{jj} \gg R_j$), the EDTI growth rate is given by the following expression which is deduced from Eq. (2.27):

$$\lambda = \chi_j (q_{R\varepsilon}^2 - q^2 - \tau_{j0}^{-1} / \chi_j). \qquad (2.30)$$

Allowing for Eq. (2.29), we find that Eq. (2.17) yields an expression for the amplitude of strain on the surface in Eq. (2.10) at time t:

$$A = A(q,t) = -\frac{\lambda^2 f_j Y_{j1}(t=0)}{(\chi_j q^2 + \tau_{j0}^{-1})\,\Phi c_1^2 (1-\beta)},$$

where λ is given by Eq. (2.30) (if $\varepsilon_{jj} \gg R_j$, the function Φ of the system (2.17) is independent of q); allowing for Eq. (2.10), we find that the resultant strain on the surface at the end of a laser pulse $t = \tau_p$ is

$$\xi(x, \tau_p) = \sum_q A(q, \tau_p) \exp\left(iqx + \int_0^{\tau_p} \lambda dt \right).$$

The strain correlation function is

$$\langle \xi^2(x) \rangle = \sum_q \langle A^2(q, \tau_p) \rangle \exp\left(2\int_0^{\tau_p} \lambda dt\right)$$

$$\sim \int_0^\infty dq \langle A^2(q, \tau_p) \rangle \exp(2\lambda\tau_p) \sim \int_0^\infty \xi_q^2 dq,$$

where the spectral strain function is

$$\xi_q^2 \sim \left(\frac{q_{R\varepsilon}^2 - q^2 - \tau_{j0}^{-1}/\chi_j}{q^2 + \tau_{j0}^{-1}/\chi_j}\right)^4 \exp(2\lambda\tau_p),$$

and λ is given by Eq. (2.30). The value $q = q_{max}$ at which the maximum of the spectral function is attained at time $t = \tau_p$ determines, under linear conditions, the period of a grating in the case when $\varepsilon_{jj} \gg R_j$. For example, in the DTI case ($\tau_{j0}^{-1} = 0$), we have

$$q_{max} = q_{R\varepsilon}, \text{ for } q_{R\varepsilon} > (4\tau_p\chi)^{-1/2}, \quad (2.31a)$$

$$q_{max} = (4\tau_p\chi)^{-1/2}, \text{ for } q_{R\varepsilon} < (4\tau_p\chi)^{-1/2}. \quad (2.31b)$$

If we calculate the critical intensity necessary for the EDTI (found from the condition $\lambda = 0$) by expanding Eq. (2.22) in terms of the parameters $\lambda / c_{t,l} q$, $(\lambda + \tau_{j0}^{-1}) / \chi_j q^2 \ll 1$, we then obtain a soft relaxation mode:

$$\lambda = -(2\chi_j q^2 + \tau_{j0}^{-1}) + \frac{2q}{\gamma_0}\left(\frac{R_j}{1-\beta} + \varepsilon_{jj}\right), \quad (2.32)$$

where R_j is given by Eq. (2.17) and ε_{jj} by Eq. (2.5).

In the case of the EDI from Eq. (2.32) we obtain a soft carrier-density mode

$$\lambda = -(2D_e q^2 + \tau^{-1}) + \frac{4q|\mathbf{E}|^2}{\gamma_0 \pi \hbar^2 \varepsilon'} \frac{\partial \varepsilon''}{\partial \omega} \times \left[\left|\frac{\partial E_g}{\partial n_e}\right| + \frac{\theta^2}{(1-\beta)\rho c_l^2}\right]. \quad (2.33a)$$

We can therefore see that the EDI appears only when the condition $\partial\varepsilon'' / \partial\omega > 0$ is satisfied. This condition is obeyed by various semiconductors in the range of frequencies of generally available lasers. In the case of DTI, we can deduce from Eq. (2.32) a soft temperature mode:

$$\lambda = -2\chi q^2 + \frac{4q|\mathbf{E}|^2 \omega}{\gamma_0 \pi \hbar \varepsilon' c_v} \frac{\partial \varepsilon''}{\partial \omega}\left[\left|\frac{\partial E_g}{\partial T}\right| + \frac{\theta K \alpha}{(1-\beta)\rho c_l^2}\right]. \quad (2.33b)$$

We can see that the DTI can be achieved for different signs of $\partial\varepsilon'' / \partial\omega$ depending on the sign of θ and on the relative magnitudes of the first and the second terms in the brackets of Eqs. (2.33). The condition $\lambda = 0$ in Eqs. (2.33a) and (2.33b) yields the critical intensity E_{cr}^2 for the appearance of the ETI and DTI, respectively.

Therefore, it follows from this section that if $|\mathbf{E}|^2 > E_{cr}^2$ the specific Fourier amplitudes of coupled fields of static strain (Eq. (2.18)) and of the nonequilibrium carrier density, and temperature (Eq. (2.12)) develop on the surface exponentially with time and the process is characterized by the growth rate λ_{max} (Eq. (2.28b)). Consequently, in the linear EDTI case we can expect structures in the form of one-dimensional gratings (Fig. 2) with a period

$$d = 2\pi / q_{max}, \quad (2.34)$$

where, in the case $R_j \gg \varepsilon_{jj}$, the value of q_{max} is given by Eq. (2.28a), while for $R_j \ll \varepsilon_{jj}$, it is given by Eq. (2.31).

2.4. Laser-Induced Semiconductor-Metal Phase Transition Involving Superstructure Formation

We consider the nonlinear case for the EDI stabilized by the nonlinear Auger recombination. The functions of interest are described at $z = 0$ by $n_1(0) = n_q \exp(iqx)$, $\xi_1(0) = \xi_q \exp(iqx)$, and $T_1(0) = T_q \exp(iqx)$, where $E_g(0) = E_{g0} + E_{g1}\exp(iqx)$. Under a steady-state condition ($\lambda = 0$) near the threshold ($|\mathbf{E}|^2 \geq E_{cr}^2$) the substitution $\tau_n^{-1} = \tau^{-1} + \gamma_A |n_q|^2$ into Eq. (2.32) gives

$$n_1(0) = |n_q| - \frac{1}{\gamma_A^{1/2}}\left[\frac{2q}{\gamma_0}\left(\frac{R_n}{1-\beta} + \varepsilon_{nn}\right) - 2D_e q^2 - \tau^{-1}\right]^{1/2}. \quad (2.35)$$

The threshold for appearance of the steady-state values of n_g corresponds to E_{cr}^2 and naturally coincides with the EDI threshold of Eq. (2.33a). Far from the threshold ($|\mathbf{E}|^2 \gg E_{cr}^2$) we similarly obtain from Eq. (2.27)

$$n_q = \frac{1}{\gamma_A^{1/2}}\left\{D_e\left[\left(\frac{(q+q_{R\varepsilon})^2}{4} + qq_R\frac{2\beta}{1-\beta}\right)^{1/2} + \frac{q_{R\varepsilon} - q}{2}\right]^2 - D_e q^2 - \tau^{-1}\right\}. \quad (2.36)$$

Therefore, the dependence of n_q on q repeats the dependence $\lambda = \lambda(q)$. Eqs. (2.10) and (2.12) yield the amplitude of a steady-state deformation wave on the surface

$$\xi_q = n_q(D_e\gamma_0\delta_n - \varepsilon_{nn}) / \varepsilon_{n\xi}, \quad (2.37)$$

where $\delta_n = [q^2 + (\tau^{-1} + \gamma_A n_q^2) / D_e]^{1/2}$, while the amplitude of a steady-state temperature wave is

$$T_q = \frac{\varepsilon_{T\xi} D_e \delta_n}{\varepsilon_{n\xi}\chi q} n_q.$$

Let us obtain from Eq. (2.37) a more explicit formula for the deformation Fourier harmonic amplitudes n_q

and ξ_q at $q = q_{max}$ and $\lambda = \lambda_{max}$. Using values given in Sec. 2.6 for the case of picosecond excitation ($I \sim 10^9$ W·cm^{-2}, $\tau_p = 10^{-11}$ s) for the parameters entering the expressions for δ_n (2.13) and n_q (2.36) we have $\delta_n \approx q_{max}$ and

$$n_{q_{max}} \simeq \lambda_{max}^{1/2} \gamma_A^{1/2}. \tag{2.37a}$$

Then, using Eq. (2.6a) we have $\varepsilon_{nn} \gg D_e \gamma_0 \delta_n$ so that from Eq. (2.37) $\xi_{q_{max}} = n_{q_{max}} \varepsilon_{nn} / \varepsilon_{n\xi}$ whence

$$\xi_{q_{max}} \simeq \frac{\lambda_{max}^{1/2}}{\gamma_A^{1/2}} \frac{\beta_n}{\theta}. \tag{2.37b}$$

Here λ_{max} is given by Eq. (2.28b).

If the Auger recombination is unimportant (for example in the case on the time scale of 10^{-13} s, i.e., during the femtosecond pulse duration ($(\tau_p \sim 10^{-13}$ s, $I \sim 10^{11}$ W·cm^{-2}), see Sec. 2.7)) then the EDI stabilization occurs due to the acousto-optic nonlinearity. In this case, the nonlinear regime of EDI in the bulk of the semiconductor was considered in Ref. [41]. Here we outline the derivation of Ref. [41] and present the results. We represent the strain corresponding to the Fourier harmonic with $q = q_{max}$ and $\lambda = \lambda_{max}$ in the form

$$\xi = \xi_{q_{max}} \exp(-iq_{max}x) + \text{c. c.}$$

Then we expand ε'' similarly to Eq. (2.5) but now we take into account the cubic term $\xi_{q_{max}}$, aside from the linear one with respect to $\xi^3_{q_{max}}$. Then from Eq. (2.3b) we find the stationary solution for the harmonic amplitude

$$n_e = n_{q_{max}} \exp(-iq_{max}x) + \text{c. c.}$$

and from Eq. (2.4) we have the connection

$$n_{q_{max}} = -c_l^2 \rho \xi_{q_{max}} / \theta.$$

From the above two connections, we find the Landau type equation for the order parameter $\xi_{q_{max}}$

$$\xi_{q_{max}} \left(1 - \frac{R_n}{\Gamma_{max}}\right) = \frac{R_n}{6\Gamma_{max}} \frac{\theta^2}{\hbar^2} \frac{\partial^3 \varepsilon'' / \partial \omega^3}{\partial \varepsilon'' / \partial \omega} \xi^3_{q_{max}},$$

$$\Gamma_{max} = D_e q^2_{max},$$

where the pump parameter $R_n \sim |\mathbf{E}|^2$ is given in Ref. [41]. From this equation we obtain

$$|\xi_{q_{max}}| = \frac{\hbar}{|\theta|} \left| \frac{6\partial \varepsilon'' / \partial \omega}{\partial^3 \varepsilon'' / \partial \omega^3} \right| \left(1 - \frac{\Gamma_{max}}{R_n}\right)^{1/2}.$$

At $\varepsilon'' = \text{const}(\omega - E_g / \hbar)^{3/2}$ we find for the order parameter

$$\xi_{q_{max}} = 5(\hbar\omega - E_g)\left(1 - \frac{\Gamma_{max}}{R_n}\right)^{1/2} / |\theta|.$$

Thus upon high exceeding of the threshold ($R_n \gg \Gamma_{max}$) the amplitude of the deformation wave is

$$\xi_{q_{max}} = 5(\hbar\omega - E_g) / |\theta|. \tag{2.37c}$$

This equation is used for the evaluation of strain in EDI under femtosecond excitation in Sec. 2.7.

We now substitute Eq. (2.37) and the value of T_q in Eq. (2.1). Then, a wave of the renormalized band gap at $z = 0$ is obtained using an expression for ε_{nn} given by Eq. (2.6a) on the assumption that $|\mathbf{E}|^2 > E^2_{cr}$ is described by

$$E_g(0) = E_{g0} - E_{g1}(q) \cos qx,$$

$$E_{g1}(q) = D_e \delta_n n_q \left(\varepsilon' \pi \hbar^2 \gamma_0 / 2 \frac{\partial \varepsilon''}{\partial \omega} |\mathbf{E}|^2 + \frac{\hbar\omega}{\chi q c_v} \left| \frac{\partial E_g}{\partial T} \right| \right). \tag{2.38}$$

Note that the term β_n in Eq. (2.1) is balanced exactly by a part of the second term on the right-hand side of Eq. (2.37), i.e., effective renormalization in Eq. (2.38) occurs only due to the deformation and temperature waves. When the modulation amplitude in Eq. (2.38) obeys $E_{g1} \geq E_{g0}$, we find that a grating appears on the surface, which represents alternating metallic and semiconductor phases. In the case $R_j \gg \varepsilon_{jj}$ the period of this grating is given by the value of q_{max} of Eq. (2.28). In the opposite limit of $R_j \ll \varepsilon_{jj}$ the maximum, n_q in Eq. (2.36) is attained at $q = 0$. Then, in Eq. (2.38) we can sum over the surface modes:

$$\begin{aligned} E_g(0) &= E_{g0} - \sum_q E_{g1}(q) \cos(qx) \\ &\equiv E_{g0} - [E_{g1}(x)]_{eff}. \end{aligned} \tag{2.39}$$

It follows from Eq. (2.36) and the condition $\varepsilon_{jj} \gg R_j$ that $n_q \propto (q^2_{R\varepsilon} - q^2)^{1/2}$, and using Eqs. (2.39) and (2.38), where $\gamma_A n_q^2 \gg q^2 D_e$ and the second term in parentheses is retained, we obtain that

$$[E_{g1}(x)]_{eff} = \int_0^{q_{R\varepsilon}} dq \cos(qx)(q^2_{R\varepsilon} - q^2) \sim \sin(q_{R\varepsilon}x). \tag{2.40}$$

Therefore, for $\varepsilon_{jj} \gg R_j$, a grating with a period $d = 2\pi / q_{R\varepsilon}$ forms in the nonlinear EDTI case.

In addition to instability of the Fourier amplitudes with $q \neq 0$ in the EDTI, the amplitudes of the deformation (strain), carrier density, and temperature fields for $q = 0$ also increase exponentially in time, which gives rise to a spatially homogeneous reduction of E_g, i.e., it increases the optical absorption coefficient. This could account for the experimental observation of a strong reduction in the optical absorption length in semiconductors at a high rate of excitation with light characterized by a photon energy $\hbar\omega$ much larger than E_g [37].

2.5. Formation of Radial-Ring Electron-Strain Structures

Let us assume that the laser field has axial symmetry (relative to the z-axis). We seek a simultaneous solution of the system of Eqs. (2.4), (2.7), and (2.8) subject to the boundary condition (2.9) written in cylindrical coordinates, ignoring at first the dependence of $\mathbf{E}$ on r in Eq. (2.2) (the influence of the dependence of the laser field on the coordinate r will be discussed later). The solution of the problem in cylindrical coordinates follows the procedure of Sec. 2.3, provided that we make the substitution $\exp(iqx) \to J_m(qr)\cos m\varphi$ in the expressions of Eq. (2.10) where J_m is the Bessel function of the first kind of the order m, and m is an integer (the star structure, see Fig. 2). We then find that the components of the displacement vector ($\alpha = r, \varphi, z$) are given by

$$U_\alpha = (a_\alpha N \exp(-\kappa_t z) + b_\alpha M \exp(-\kappa_l z) + M \sum_{j=n,T} c_{\alpha j} \Phi_j \exp(-\delta_j z)) \Psi_\alpha \exp\left(\int_0^t \lambda dt\right), \quad (2.41)$$

where

$$a_z = q,\ a_\varphi = -a_r = \kappa_t,\ b_z = \kappa_l,\ b_\varphi = -b_r = q,$$

$$c_{zj} = -\lambda^2,\ c_{rj} = -c_{\varphi j} = \lambda^2 q/\delta_j.$$

$$\Psi_z = J_m(qr)\cos m\varphi,$$

$$\Psi_r = \frac{1}{2}[J_{m-1}(qr) - J_{m+1}(qr)]\cos m\varphi,$$

$$\Psi_\varphi = \frac{1}{2}[J_{m+1}(qr) + J_{m-1}(qr)]\sin m\varphi.$$

The dispersion equation for the EDTI deduced from the boundary conditions for $\mathbf{U}$ and from Eq. (2.41) is exactly identical with Eq. (2.22). Therefore, the expressions for q_{max} and λ_{max} (Eqs. (2.28a) and (2.28b)), which separate the dominant structure in the linear regime, are valid also in the case of the radial-ring structures under consideration.

It is clear from Eq. (2.22) that surface harmonics with any value of m are characterized by the same growth rate. This degeneracy in m is a consequence of neglecting the dependence of the laser field $\mathbf{E}^2$ intensity on r in Eq. (2.2).

We can find the parameters m by solving the problem of the growth of the EDTI, assuming a Gaussian transverse distribution of laser intensity. Consider, for example, another possible class of surface structures in the form of radial rays (Fig. 2).

Let us assume that the pump field has a Gaussian intensity distribution

$$|\mathbf{E}|^2 = E_0^2 \exp(-r^2/r_0^2). \quad (2.42)$$

Then, Eq. (2.8) becomes

$$\frac{\partial Y_{j1}}{\partial t} + \Delta_j Y_{j1} = (\varepsilon_{j\xi}\xi_1 + \varepsilon_{jn}n_1 + \varepsilon_{jT}T_1)|_{z=0} \times \exp(-\gamma_0 z - r^2/r_0^2), \quad (2.43)$$

where $\varepsilon_{j\xi}$, ε_{jn}, and ε_{jT} are given by expressions in Eq. (2.6a), provided we replace $|E|^2$ with E_0^2. The boundary conditions for Y_{j1} remain the same. We specify ξ_1 and Y_{j1} at $z = 0$ in the form

$$\xi_1 = A\left(\frac{r}{r_0}\right)^m \exp\left(-\frac{r^2}{r_0^2}\right)\cos(m\varphi)\exp\left(\int_0^t \lambda dt\right), \quad (2.44)$$

$$Y_{j1} = A_j(t)\left(\frac{r}{r_0}\right)^m \exp\left(-\frac{r^2}{r_0^2}\right)\cos(m\varphi)\exp\left(\int_0^t \lambda dt\right). \quad (2.45)$$

Here, as in Eqs. (2.9) and (2.10), we are using A for the initial amplitudes, and A_j are slow functions of time, where m is an integer; we shall assume that $m \gg 1$. Then a maximum of the function $(r/r_0)^m \exp(-r^2/r_0^2)$ lies at a point $r_{max} = r_0(m/2)^{1/2} \gg r_0$. In the range $r < r_0$ we can assume that $(r/r_0)^m \exp(-r^2/r_0^2) \cong (r/r_0)^m$ and Eq. (2.43) can be written as follows:

$$\frac{\partial Y_{j1}}{\partial t} + \Delta_j Y_{j1} = (\varepsilon_{j\xi}A + \varepsilon_{jn}A_n + \varepsilon_{jT}A_T)\left(\frac{r}{r_0}\right)^m \cos m\varphi \times \exp\left(-\frac{r^2}{r_0^2} - \gamma_0 z + \int_0^t \lambda dt\right). \quad (2.46)$$

The solution of Eq. (2.46) subject to the conditions $r/r_0 \ll m$ and $\gamma_0 \gg m^{1/2} r_0^{-1}$ can be obtained in the form

$$Y_{j1} = \frac{\varepsilon_{j\xi} A \exp\left(-\tilde{\delta}_j z - \frac{r^2}{r_0^2} + \int_0^t \lambda dt\right)\left(\frac{r}{r_0}\right)^m \cos m\varphi}{\chi_j \gamma_0 \tilde{\delta}_j \left(1 - \sum_{j=n,T} \varepsilon_{jj}/\chi_j \gamma_0 \tilde{\delta}_j\right)}, \quad (2.47)$$

where $\tilde{\delta}_j$ is given by Eq. (2.13), provided q^2 is replaced with $\tilde{q}^2$:

$$\tilde{q}^2 = 4(m+1)/r_0^2. \quad (2.48)$$

Using Eq. (2.4) and the boundary conditions for the vector $\mathbf{U}$ in cylindrical coordinates, and following the solution procedure similar to that described in Sec. 2.3, and also allowing for the solutions Y_{j1} described by Eq. (2.47) and the conditions subject to which the solu-

tion of Eq. (2.46) is obtained, we find that the components of the displacement vector are described by

$$U_i = \frac{r^{m-1}}{r_0^m} \exp\left(-\frac{r^2}{r_0^2} + \int_0^t \lambda dt\right) \Psi_i \left(a_i M \exp(-\kappa_t z) + b_i N \exp(-\kappa_t z) + M \sum_{j=n,T} c_{ij} \Phi_j \exp(-\delta_j z)\right), \quad (2.49)$$

where $i = z, \varphi, r$; $\Psi_r = m\cos m\varphi$, $\Psi_\varphi = -m\sin m\varphi$, $\Psi_z = r\cos m\varphi$; $a_r = a_\varphi = 1$, $a_z = -\kappa_t$; $b_r = b_\varphi = -\kappa_t$, $b_z = q$; $c_{r,j} = c_{\varphi j} = -\lambda^2 / \delta_i$, $c_{zj} = \lambda^2$.

Here, $\kappa_{l,t}$ and Φ_j are given by Eqs. (2.19) and (2.20), where q^2 is replaced with $\tilde{q}^2$ given by Eq. (2.48). The dispersion equation obtained from Eqs. (2.9) and (2.49) coincides with the dispersion equation (2.22) if q^2 is replaced with $\tilde{q}^2$, i.e., it specifies $\lambda(m)$. If the expressions for q_{max} (Eq. (2.28a) and λ_{max} (Eq. (2.28b)) are modified by replacing q^2 with $\tilde{q}^2$, they give the value of m_{max} at which λ reaches its maximum:

$$m_{max} = (q_{R\varepsilon}^2 r_0^2 / 4)\left[(5a^2 + 6a + 1)^{1/2} - (2a+1)^{1/2}\right]; \quad (2.50)$$

the value of m_{max} given by Eq. (2.50) determines the number of rays in the dominant structure.

2.6. Comparison of Theoretical and Experimental Results

As was already mentioned above, the symmetry of the structures formed as a result of the EDTI should be governed by the symmetry of the laser beam for an isotropic surface or by the symmetry of the crystal surface. We now obtain numerical estimates of the parameters and compare the theoretical predictions with experimental results. For typical values $c_v = 2 \times 10^7$ erg·cm^{-3}·K^{-1}, $K \cong 10^{12}$ erg·cm^{-3}, $\alpha \cong 2 \times 10^{-5}$ K^{-1}, $\partial\varepsilon'' / \partial\omega \cong 10^{-15}$ s, $|\theta| \cong 10^{-11}$ erg, $\rho \cong 5$ g·cm^{-3}, $c_1 = 5 \times 10^5$ cm·s^{-1}, $\beta = 0.4$, $\omega \cong 4 \times 10^{15}$ s^{-1}, $|\partial E_g / \partial T| \cong 4 \times 10^{-4}$ eV·K^{-1}, $|\partial E_g / \partial n_e| = 10^{-32}$ erg·cm^3, $\chi = 0.1$ cm^2·s^{-1}, $\gamma_0 = 10^5$ cm^{-1}, $\gamma_A = 4 \times 10^{-31}$ cm^6·s^{-1}, $\hbar\omega \cong 1$ eV, $D \cong 10^2$ cm^2·s^{-1} we find from Eq. (2.17) that $R_T \sim R_n \sim \varepsilon_{nn} \sim \varepsilon_{TT} \sim 10^4 - 10^5 |\mathbf{E}|^2$ esu. We find from Eq. (2.33b) that the critical intensity for the appearance of the DTI is $I_{cr} \cong 2 \times 10^6$ W·cm^{-2} when $q \cong 10^4$ cm^{-1}. The critical intensity for the EDI is $(D_e / \chi)\hbar\omega|\partial E_g / \partial T| / (c_v|\partial E_g / \partial n_e|) \cong 10$ times larger. It follows from Eq. (2.28) that in the EDI case we have $q_{max} \sim q_{R\varepsilon} \sim 10^{-2}|\mathbf{E}|^2$ esu $\cong 10^4 - 10^5$ cm^{-1} for $I = 6 \times 10^8$ W·cm^{-2}, i.e., the period d of the structures is of the order of 1 - 5 μm. Eq. (2.28b) yields $\lambda_{max} \sim D_e q_{max} \sim 10^{10} - 10^{11}$ s^{-1} for the growth rate. The amplitude of the renormalization E_g for the above values of the parameters is $E_{gl} \cong 1$ eV, i.e., the EDTI can result in the insulator-metal phase transition. This conclusion and estimates of the structure periods as well as their growth times are in agreement with the experimental results reported in Ref. [37], where laser pulses of $\tau_p = 5 \times 10^{-11}$ s duration were used. It was found that gratings of alternating metal and semiconductor phases or "star"-like structures were formed on an isotropic surface of VO_2, depending on the symmetry of the laser field. It follows from Eq. (2.50) that for $r_0 \sim 5 \times 10^{-3}$ cm [37], the number of rays in the "star"-like structure can be as large as $m = 50$, which agrees with the experimental results (see Fig. 4); moreover, we have $\lambda_{max}\tau_p \sim 5 > 1$.

It is clearly seen from Fig. 4b that the number of rays increases with the distance from the center of the irradiated spot. This increase occurs as a ray bifurcation. A similar phenomenon is observed in the case of vacancy GDI of Sec. 4.1 (compare Figs. 4b and 11). This phenomenon is explained in Sec. 4.1 (see Fig. 12).

These estimates allow us to justify the boundary conditions given in Eq. (2.7). If we use Eq. (2.17), we find from Eq. (2.12) an expression for $(\partial Y_{j1}/\partial z)|_{z=0}$ and from Eq. (2.18) an expression for $U_z(0)$. We shall assume that in the case of picosecond laser pulses we have $T_0(z,t) \equiv T(0,t)\exp(-\gamma_0 z)$ and $n_0(z,t) = n_0(0,t)\exp(-\gamma_0 z)$, so that in the DTI case we obtain the following estimate

$$\frac{\partial^2 T_0}{\partial z^2} U_z|_{z=0} \Big/ \frac{\partial T_1}{\partial z}\Big|_{z=0} \sim (\gamma_0^2 \chi \lambda^{-1})\,[K\alpha T_0(0)]/\rho c_l^2 \sim 10^{-4},$$

whereas in the EDI case, the corresponding estimate gives

$$\frac{\partial^2 n_0}{\partial z^2} U_z|_{z=0} \Big/ \frac{\partial n_1}{\partial z}\Big|_{z=0} \sim (\gamma_0^2 D_e \lambda^{-1})\,[\theta n_0(0)]/\rho c_l^2 \sim 10^{-1}$$

for $n_0(0) \sim 10^{21}$ cm^{-3}, which confirms the validity of the boundary conditions given by Eq. (2.7) for the case in question.

In the experiments described in Ref. [79], a (111) surface of crystalline silicon was irradiated with laser pulses of wavelength $\lambda = 0.53$ μm, creating one-dimensional gratings of the surface relief in which the lines were parallel to one of the [110] axes. The dependence of the grating orientation on the crystallographic axes indicated that a deformation mechanism was responsible for the formation of these structures. The structure period was independent of λ, angle of incidence, and polarization of the incident radiation, but was governed by the pulse duration. It was found that $d_1 \cong 3 \times 10^{-5}$ cm for $\tau_{p1} = 10^{-11}$ s, whereas $d_2 \cong 6 \times 10^{-6}$ cm for $\tau_{p2} = 5 \times 10^{-12}$ s, i.e., the relationship $(d_1 / d_2) \cong (\tau_{p1} / \tau_{p2})^{1/2}$ was obeyed. In the case of Si, one has $\varepsilon_{nn} / R_n \sim 10$, so that the period of the EDTI structures should be given by Eq. (2.31b), i.e., $d \sim \tau_p^{1/2}$, which is in agreement with the experimental result of Ref. [157].

We note that apart from the periodic surface structures formed due to the EDTI development, qualitatively different surface structures are also formed under pulsed laser irradiation of the semiconductors

(see Sec. 4.3.1). These interference structures of modulation of the surface relief with the periods $d \propto \lambda_L$, where λ_L is the excitation light wavelength, may appear because of the diffraction of the incident wave from the surface relief. We can describe these structures by including interference sources of the EE_1 type in the right-hand side of Eq. (2.4), where $E_1 \sim U_{1z}|_{z=0}$ is the amplitude of the diffracted wave. These structures appeared in the solid phase due to the interference instability of sublimation or due to generation of coupled diffracted waves and surface acoustic waves (see Refs. [24 - 26]). The growth rates of the interference instability as a function of q have very narrow maxima (see Refs. [25, 26]), the positions of which are generally different from the positions of maxima of the EDTI growth rates, so that we can regard these instabilities as being independent in different ranges of q. Therefore, we ignore the contribution of interference sources in Eq. (2.4) when considering the EDTI (excellent reviews of the experimental and theoretical investigations of the interference surface instabilities are given in Refs. [22, 23]).

In contrast to the interference instability case, the characteristic scale of the structure formed because of the EDTI is not governed directly by the wavelength λ_L, and its geometry is not generally related to polarization of the incident radiation, so that these two types of structures are easily distinguished experimentally (see Sec. 4.3.1).

2.7. Superfast Phase Transition to Centrosymmetric Crystalline State in GaAs under Femtosecond Laser Excitation

There was great interest in the past few years in the nature of phase transitions on the surface of solids under pulsed femtosecond laser excitation [4 - 9]. When the pulse duration is comparable to or less than the characteristic time of electron-phonon relaxation in solids, principally new mechanisms of phase transitions may be involved. One indication of ultrafast phase transition on the Si surface under 100-fs pulsed laser excitation was revealed in Ref. [7] with the use of time-resolved linear and second-harmonic reflection.

In recent experiments [8] the temporal behavior of linear and nonlinear optical reflection from the GaAs surface under 100-fs pulse laser excitation was observed, which gave evidence of the ultrafast phase transition to the structurally new phase with properties different both from that of the initial crystal and that of melted material. The transition occurs on a time scale of about 100 fs, which is approximately one order of magnitude shorter than the time required for the electron relaxation to the bottom of the conduction band, the latter time being discussed in numerous experimental and theoretical studies [5, 7, 45, 46]. Therefore, such a kind of phase transition cannot be considered as conventional melting following energy transfer from excited electrons to the lattice, and principally different mechanisms should be analyzed. In this section we present the phenomenological model [47] describing in a self-consistent manner the ultrafast dynamics of linear and nonlinear optical reflection from the GaAs surface observed in Ref. [8]. It infers initial ultrafast transition to the nonequilibrium crystalline semiconductor phase with centrosymmetric lattice structure, which exists only during the first picosecond after excitation and is followed by melting of the subsurface layer due to energy transfer to the lattice and its heating up to the normal melting point.

It was found in Ref. [47] that the structural phase transition is possible under high electron plasma density and laser-induced stress in the subsurface layer achievable during strong femtosecond laser excitation due to the development of the EDTI. Analysis of lattice dynamics under laser excitation based on the equation for the amplitude of the zone-edge TA-phonon mode, reveals the time required for such phase transition to be consistent with the value observed experimentally. In doing so, laser irradiation is assumed to induce coherent shift of atoms from their initial positions to new quasi-equilibrium positions in a centrosymmetric lattice, rather than the increase of amplitude of their random vibrations corresponding to the increase of lattice temperature.

The experiments [8] utilized high structural sensitivity of the Second Harmonic Generation (SHG) in reflection from the surface, in order to study the dynamics of phase transition in a GaAs subsurface layer under 100-fs laser excitation. A GaAs crystal is a noncentrosymmetric material (symmetry class 43m) and hence exhibits strong second-order optical nonlinearity $\chi^{(2)}$ in the electric dipole approximation. Therefore, laser-induced phase transition to any phase with centrosymmetric structure (crystalline, or disordered or melted) is expected to cause an abrupt decrease of the SH intensity. In the centrosymmetric phase the second-order susceptibility is nonzero only in the electric quadrupole approximation, thus yielding a value of the susceptibility several orders of magnitude less than that in the electric dipole approximation.

Note that symmetry relations governing the nonlinear susceptibility, relay to the long-range order with the characteristic length comparable to the laser wavelength. In contrast, linear reflectivity of cubic crystals is determined by the band structure and therefore relays to the short range order within a few coordination spheres.

Pump-and-probe experiments [8] revealed the complicated dynamics of linear and nonlinear reflection from GaAs at laser fluence three times that of the melting threshold. The linear reflectivity measurements reveal more gradual rise with a characteristic time of 1 ps up to the value characteristic of molten (metal-like) material. In contrast, SH reflection demonstrates an abrupt decrease with a characteristic time of about 100 fs followed by additional fast changes in the first picosecond and eventual onset of a low constant value.

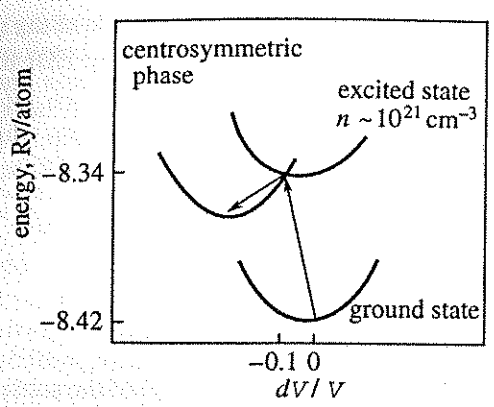

Fig. 6. *Energy diagram of GaAs. The arrows denote ultrafast transition to a new centrosymmetric phase, achieved via an excited state of GaAs.*

The SH dynamics imply the structural phase transition to the centrosymmetrical state, still semiconductor-like during the first picosecond after excitation, as is seen from the behavior of linear reflectivity. Therefore, the problems which should be resolved are the following: (1) what is the nature of the state of the material existing in the first picosecond after excitation and (2) how can the phase transition to this state occur on a time scale of about 100 fs? Obviously, the second problem cannot be resolved assuming lattice heating through spontaneous emission of phonons by photoexcited electrons, because the latter process takes at least several hundred femtoseconds.

There are principally two possibilities regarding the structure of the short-lived state of GaAs in the first picosecond after laser excitation. Since SH is sensitive to the long-range order, the fast drop of the reflected SH might be due to the loss of crystalline order over the distance of approximately the laser wavelength, while the short-range order on the scale of two first coordination spheres remains approximately unchanged, and thus the material remains a semiconductor. This situation meets the major conditions of the "cold melting" hypothesis, which implies lattice disordering [7].

A principally different possibility was considered in Ref. [47], in which the observed drop of the SH intensity is attributed to a transition to crystalline centrosymmetrical state which exists only during the first picosecond after excitation. It is shown that the time necessary for such a kind of transition is not limited by the characteristic time of spontaneous electron-phonon relaxation, and can be of the order of 100 fs.

It is known that in an equilibrium state, covalent (Si, Ge) and ion-covalent (GaAs, ZnO, InP, InSb) semiconductors undergo phase transitions to new phases (characterized by β-tin, NaCl or orthorhombic structure) when the applied pressure exceeds certain critical values [48]. In GaAs the transition into the orthorhombic semiconductor phase occurs at the lowest value of reduction of the relative crystal cell volume $dV/V = -0.17$ (in Si the transition to β-tin structure occurs at $dV/V = -0.32$). In highly excited semiconductors, phase transition can occur at lower pressures, and the nature of the final phase may change. Thus, it was shown theoretically in Ref. [49] that at the electron-hole plasma concentration of $n = 10^{22}$ cm^{-3} and electronic temperature $T = 10^4$ K, GaAs undergoes a phase transition into a metal-like centrosymmetric phase possessing symmetry similar to that of NaCl at $dV/V = -0.1$ (see Fig. 6). It will be shown below that GaAs can undergo ultrafast phase transition to a new phase with lattice symmetry different from the initial one under excitation by a strong femtosecond laser pulse realized in the experiment of Ref. [8]. Using phenomenological description of the laser induced phase transition, the dependence of the fundamental bandgap E_g of a semiconductor on the modulus of the relative change of crystalline lattice cell $|dV/V| = \xi$, and the electron-hole plasma concentration n_e can be written as (compare (2.1)):

$$E_g = E_{g0} - \theta\xi - \beta_n n_e, \qquad (2.51)$$

where E_{g0} is the equilibrium fundamental bandgap, $\beta_n > 0$ and θ is the interband deformation potential. Note that in Eq. (2.51) we neglected the bandgap renormalization due to laser-produced heating, which is insignificant on the time scale of $t = 10^{-13}$ s under consideration. At $E_g = E_{g1}$ the crystal undergoes a phase transition to a new semiconductor-like phase, and at $E_g = 0$ – to a metal-like phase. Thus, the lines $E_g = E_{g1}$ and $E_g = 0$ divide the (n_e, ξ)-plane into three regions: the initial semiconductor-like phase (S_0), the new laser-induced semiconductor-like phase (S_1) and solid metal-like phase (S_M) (Fig. 7). In particular, it may occur that $E_{g1} = 0$ and thus only semiconductor-metal phase transition takes place. The initial equilibrium state corresponds to the zero point of this diagram. The excitation pulse creates plasma with density of about $n_e = 10^{22}$ cm^{-3} and lattice deformation of the order of $\xi = 0.1$ (see below). The critical values n_{cr} and ξ_{cr} correspond to intersection of the initial semiconductor-like phase energy curve with that of the new semiconductor

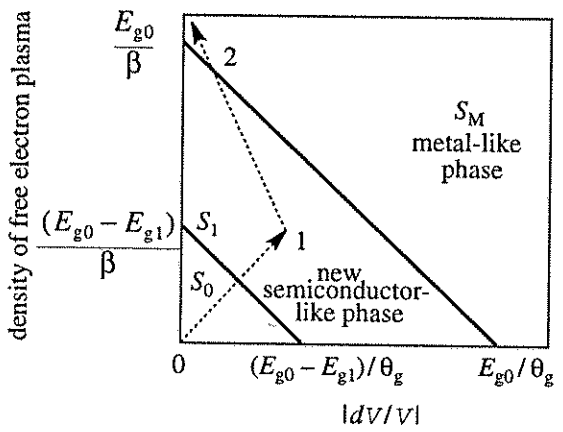

Fig. 7. *Schematic phase diagram of GaAs. The dotted line shows ultrafast transition from the initial state (0) to the centrosymmetric crystalline state (1) and the subsequent slower onset of the melt (2).*

($E_{g1} \neq 0$), or metal ($E_{g1} = 0$) phase at the energy diagram of Fig. 6. It is at this point that the transition to a new symmetry takes place. This phase transition occurs as a displacing type II phase transition due to softening of the optical or acoustic phonon mode. It was shown in Ref. [50], for example, that under excitation of a dense ($n_e > 10^{21}$ cm^{-3}) plasma the TA-acoustic mode at the edge of the Brillouin zone becomes unstable first. We assume that the amplitude of this unstable phonon mode obeys the following equation

$$\partial^2 Q/\partial t^2 + \omega_0^2 (1 - \theta_1 \xi - \beta_{n1} n_e) Q = -b|Q|^2 Q \tag{2.52}$$

and plays the role of the order parameter of this laser-induced displacing phase transition, where b is the phonon anharmonicity constant,

$$\beta_{n1} = \beta_n (E_{g0} - E_{g1})^{-1}, \quad \theta_1 = \theta (E_{g0} - E_{g1})^{-1}.$$

From Eq. (2.52) we have that the stationary state (new nonequilibrium phase) with the displacement

$$|Q| = (\omega_0^2/b)^{1/2} (\theta_1 \xi + \beta_{n1} n_e - 1)^{1/2} \tag{2.53}$$

is established in the time interval of

$$t = \omega_0^{-1} (\theta_1 \xi + \beta_{n1} n_e - 1)^{-1/2}. \tag{2.54}$$

Let us make numerical estimates. The number density of plasma generated on the surface layer of the semiconductor by the end of the pulse (without taking into account diffusion and Auger recombination; both are unimportant on a time scale $t = 10^{-13}$ s) is $n_e = \gamma(1 - R)W/\hbar\omega$, where the absorption coefficient of exciting radiation $\gamma = 4 \times 10^4$ cm^{-1}, reflection coefficient $R = 0.3$, and pulse energy density $W = 0.2$ J·cm^{-2}, $\omega = 3 \times 10^{15}$ s^{-1}. With these parameters we have $n_e = 2 \times 10^{22}$ cm^{-3}. Let us now estimate deformation of the subsurface layer. The light pressure yields the compression with $\xi = \hbar k n / \tau_p K = 4 \times 10^{-3}$, where $k = 2\pi/\lambda$, $K = 5 \times 10^{11}$ erg·cm^{-3} is the bulk elasticity modulus of GaAs. The excitation of electron-hole plasma with concentration $n_e = 10^{22}$ cm^{-3} leads to the crystal dilation $\xi = \sigma_e n_e = 2 \times 10^{-2}$, where $\sigma_e = 2 \times 10^{-24}$ cm^3 is the relative increase of the crystal volume accompanying generation of a single electron-hole pair.

The theory of electron-deformational instability (EDI) in the case of interband transitions in semiconductors (see Sec. 2.4) predicts ultrafast ($t = 10^{-13}$ s) formation of the surface grating of the plasma concentration n and coupled surface strain grating $\xi_{q_{max}}$ with the period d, given by Eq. (2.34), of the order of 10^{-5} cm ($W = 0.2$ J·cm^{-2}) and amplitude $\xi_{q_{max}}$ – see Eq. (2.37c)

$$\xi = \xi_{q_{max}} = \cos 2\pi x/d,$$

$$\xi_q \simeq (\hbar\omega - E_g)/|\theta|,$$

where x is the coordinate along one of the crystallographic axes of the surface layer.

For $(\hbar\omega - E_g) = 1$ eV, $|\theta| = 10$ the amplitude of the strain grating is $\xi_{q_{max}} = 0.1$. It follows from the EDI theory that this grating penetrates from the surface into the bulk at a distance of the order of $d = 10^{-5}$ cm, which is equal approximately to the SH absorption length. After the end of the pulse the grating disappears with a characteristic time $t = d^2/D_e = 10^{-13}$ s, where $D_e = 10^3$ cm^2·s^{-1} is the diffusion coefficient of the nonequilibrium carriers under strong laser excitation.

Thus, it is seen that femtosecond laser pulses used in the experiment can create dense plasma ($n_e = 10^{22}$ cm^{-3}) in highly compressed regions ($\xi = 0.1$) of the subsurface layer. These values of n_e and ξ meet the conditions of the laser-induced structural phase transition discussed above. It follows from Eq. (2.54) that this phase transition has a characteristic time $t < \omega_0^{-1} = \omega_{TA}^{-1} = 10^{-13}$ s, where ω_{TA} is the transverse acoustic phonon frequency at the edge of the Brillouin zone.

Thus, we see that both the threshold condition of the phase transition and the requirement of its being sufficiently fast may be satisfied in experiments [8]. The above analysis leads to the conclusion that during the action of a powerful femtosecond laser pulse, the grating of alternating different phases S_0, S_1 (or S_0, S_M) is formed with the period $d = 10^{-5}$ cm, which disappears when the pulse is over. If we assume that the symmetry of $S_1(S_M)$ phases is such that the value of $\chi^{(2)}$ of these phases is drastically reduced, then a strong decrease of the SHG intensity on a time scale of 10^{-13} s should be observed during the pulse, replaced by the rise of SHG immediately after the end of the pulse. If, for example, one takes $\chi^{(2)} = 0$, then the SHG intensity drops by 75%, which indeed was observed in the experiment under consideration.

Thus, the concept of ultrafast structural phase transition of GaAs into a new centrosymmetric phase can explain an ultrafast decrease of the SHG intensity observed experimentally in Ref. [8]. Note that recent results of Refs. [9, 51] are in agreement with the present model. It was found in Ref. [9] that the characteristic time of fast laser-induced phase transition in GaAs is strongly decreased with increasing the laser fluence. Indeed, Eq. (2.54) predicts the decrease of the characteristic transition time to the new crystalline phase with increasing the level of excitation (i.e., with increasing n_e and ξ). A detailed analysis which takes into account plasma dynamics and melting on a longer time scale is the subject of further theoretical studies.

3. LASER-INDUCED POINT DEFECT GENERATION IN SEMICONDUCTORS

We now proceed to the consideration of point lattice imperfections generated in semiconductors during the action of laser pulses.

As was already said in Sec. 1, pulsed laser irradiation (PLI) is currently used to induce modification of properties of the semiconductor materials [52, 53]. However, the quality of the laser treatment is often lim-

ited by generation of defects in the subsurface region of the irradiated materials [54 - 56]. Another important problem associated with light-induced point defect generation in semiconductors is the gradual degradation in semiconductor lasers and light-emitting diodes (see Sec. 5.3.1).

It was established (see Ref. [57] and references therein) that PLI of the A^4 and A^3B^5 semiconductors under the conditions of the interband absorption leads to formation of the defect centers already at laser energy densities of about $W = (0.05 - 0.1)W_m$, where W_m is the melting threshold. The mechanisms of their formation have not been elucidated completely.

One can point out the following factors, which can lead to laser-induced defect formation: heating, acoustic deformation, and local electronic excitation (EE) of the subsurface layer of a semiconductor. However, it was shown experimentally [57] that under the PLI with $W < W_m$ each of the above-mentioned mechanisms separately does not cause formation of the defects.

In Sec. 3.1 the electron-deformation-thermal (EDT) model of the laser induced defect formation is considered, which takes into account simultaneous influence of the above-mentioned factors on the thermal fluctuation rate of defect production in semiconductors.

In Sec. 3.2 the EDT theory of the laser induced defect formation in semiconductors based on EDT-rate of defect production is developed, which yields analytical formulas for dependencies of the generated defect concentration on laser fluence for different conditions. The theoretical results are compared with the experimental ones, obtained for A^4 and A^3B^5 semiconductors at $W < W_m$. In Sec. 3.4 the experimental results on formation of periodic surface defect structures in GaP under nanosecond UV PLI are interpreted in terms of EDT mechanism of defect generation, effective under the EDTI conditions.

3.1. Rate of Pulsed Laser-Induced Point Defect Production

Let a laser pulse with duration τ_p and energy of the quantum $\hbar\omega > E_g$ (E_g being the forbidden gap of a semiconductor) act on the surface $z = 0$ of the crystal (the z-axis is directed inside the crystal). As has been noted above, the action of the laser radiation leads to three effects which are important in the process of additional defect formation: heating, deformation of the subsurface layer, and local excitation of the initial centers. Let us discuss each of these factors.

A fraction of the energy of the photoexcited electron-hole pairs is transferred in the process of electron-phonon relaxation to the lattice and heats the latter. The thickness of the heated layer for the nanosecond range of laser pulse durations ($\tau_p = 10 - 30$ ns), of interest to us in this section, for the values of coefficients of the optical absorption $\gamma = 10^4 - 10^6$ cm^{-1}, is determined by the heat diffusion and usually amounts to several μm [58].

The strong rise of the temperature T (up to the melting point) leads to the thermofluctuation generation of defects [59, 60]. The local rate of thermofluctuation defect production, neglecting recombination is given by

$$G_d = \frac{\partial n_d}{\partial t} = C_d \exp(-E_{d0}/kT), \qquad (3.1)$$

where E_{d0} is the energy of the defect formation and $T = T_0 + \Delta T$, T_0 being the initial temperature and ΔT being the temperature rise. The explicit form of the constant C_d depends on the nature of the defect generation process.

The defect formation energy can be substantially reduced owing to the localization of the electronic energy at some point of the crystal [61, 62]. In A^4 and A^3B^5 semiconductors such localization is possible only at the defects in the process of the nonradiative capture or recombination of carriers [61]. All the mechanisms of defect formation stimulated by the localized EE can be divided into two groups: the mechanisms of vibrational instability and those of adiabatic instability [62]. In the first case the energy of the EE transforms into the vibrational energy of the defect, while in the second case it decreases the potential barrier of the defect transition to a new equilibrium position. Thus, the localization of the electronic excitation at some initial defect can induce the appearance of new centers, i.e., the process of defect multiplication takes place. Effectively, one can take into account the local electronic excitation by subtracting some quantity E_{ee} from the energy of the defect formation E_{d0}. The magnitude of E_{ee} is determined by the configurational diagram of the initial defect and by the peculiarities of the local vibrational excitation relaxation of this center [61, 62]. Thus, generally, it does not depend on the electron-hole plasma concentration n_e. Hence the effective energy of defect formation is

$$E_d = E_{d0} - E_{ee}. \qquad (3.2)$$

In the field of strain $\xi = \operatorname{div} \mathbf{U}$ of an isotropic or cubic crystal the energy of defect formation is (cf. Eq. (1.1)):

$$E_d = E_{d0} - E_{ee} - \theta_d \operatorname{div} \mathbf{U}. \qquad (3.3)$$

Expanding E_{d0} and E_{ee} in power series of ξ, we obtain

$$E_d = E_{d0}^0 - E_{ee}^0 - \theta_a \operatorname{div} U, \qquad (3.4)$$

where E_{d0}^0 and E_{ee}^0 are defect formation energy and energy of electronic excitation in the absence of strain (pressure) and the effective activation deformation potential

$$\theta_a = -\frac{\partial E_{d0}}{\partial \xi} + \frac{\partial E_{ee}}{\partial \xi} - \theta_d. \qquad (3.5)$$

Taking into account the three above-considered factors of laser action in Eq. (3.1), we obtain an expression for the rate of point defect production in a semiconductor under pulsed laser irradiation

$$G_d \equiv \frac{\partial n_d}{\partial t} = C_d \exp\left[-\frac{E_{d0}^0 - E_{ee}^0 - \theta_a \operatorname{div} \mathbf{U}}{kT}\right], \quad (3.6)$$

where C_d is now some function of the initial concentration of centers, localizing electronic excitations, and in general also a function of n_d.[2]

The relaxation times of surface deformation and of the electronic excitation are comparable to or less than the duration of a crystal cooling [58]. Owing to the very rapid cooling (10^{10} k·s^{-1} for $\tau_p \sim 10^{-8}$ s [58]), all three above-considered factors of defect formation under pulsed laser irradiation have a quenching character (i.e., the generated defects are "frozen in" after the end of the laser pulse).

With the increase of the number of pulses the defect recombination enters into play, and the density of the laser-induced thermofluctuation defects reaches its stationary value. The effective values of activation energy and defect deformational potential θ_a appearing in the stationary expression for n_d can be shown to be modified in comparison with Eqs. (3.2) and (3.5) by extracting similar terms due to recombination energy E_r and potential θ_r. We do not write these modifications explicitly, but simply write the stationary solution using the two phenomenological parameters E_{A0}^0 and $\theta_A = \theta_a$:

$$n_d = \text{const} \exp\left[-\frac{(E_{A0}^0 - E_{ee}^0 - \theta_A \xi)}{k(T_0 + \Delta T)}\right], \quad (3.7)$$

where

$$E_{A0}^0 - E_{ee}^0 - \theta_A \xi > 0.$$

Eq. (3.7) is similar to the usual expression for the equilibrium point defect concentration [60] and takes into account three factors of laser pulse influence. In the initial formulation of the EDT model in Ref. [63] we have taken into account only $\partial E_{d0} / \partial \xi$ in Eq. (3.5) (omitting θ_d and possible contribution $\partial E_{ee} / \partial \xi$). The authors of a similar model in Ref. [64] took into account all three terms in Eq. (3.5). Due to the unknown relative contributions of the three terms in phenomenological formula (3.5) it is impossible to envisage the resultant sign of θ_A, consequently, similar to Ref. [63], we postulate $\theta_A < 0$, and compare the consequences of this postulate with the experimental results.

It was pointed out in Sec. 2 that deformation of the subsurface layer under pulsed irradiation stems from two reasons: heating (the thermoelastic deformation [66], important only when $\tau_p > \tau_{e\text{-ph}} \sim 10^{-12}$ s) and generation of the electron-hole plasma (photostriction deformation [67, 68]). For the nanosecond excitation of electron-hole plasma, considered in this section, the density of the nonequilibrium carries reaches values of the order of 10^{20} cm^{-3} [58, 68]. Under these conditions the photostriction deformation turns out to be of the same order of magnitude as the thermoelastic deformation [70]. Because in the experiments usually the radius of the laser beam $r_0 \gg \gamma^{-1}$, one can consider the deformation as a uniaxial one:

$$\xi \equiv \operatorname{div} \mathbf{U} = \frac{\partial U_z}{\partial z}. \quad (3.8)$$

In the case of thermoelastic deformation we always have $\xi > 0$ (dilation). The sign of the photostriction deformation depends on the structure and excitation of the semiconductor energy bands: dilation ($\xi > 0$) in the case of Ge and GaAs [70] and compression ($\xi < 0$) in the case of Si [67].

3.2. The Electron-Deformation-Thermal Theory of Point Defect Generation in Semiconductors

To determine the number of defects formed as a result of action of the laser pulses, one must calculate the values of ΔT and ξ as functions of W and z. As we shall see in the following, for explanation of the basic experimental results it is sufficient to know the values of ΔT and ξ on the surface of the semiconductor ($z = 0$). This circumstance substantially simplifies theoretical considerations and permits one to determine ξ directly from the boundary condition for the displacement vector of the medium $\mathbf{U}$ at the free boundary $z = 0$ (see Eq. (2.9):

$$\xi = \operatorname{div} \mathbf{U}_{z=0} = \frac{K_\alpha}{\rho c_l^2} \Delta T + \frac{\theta_g}{\rho c_l^2} n_e, \quad (3.9)$$

where $n_e = n_e(z)|_{z=0}$ is the carrier density at the surface $z = 0$, and θ_g is the acoustic interband deformation potential ($\theta_g > 0$ for Si and GaP and $\theta_g < 0$ for Ge and GaAs). Let us calculate now the value of ΔT and div $\mathbf{U}$ for $z = 0$ in Eq. (3.9):

(1) The laser heating of a semiconductor surface.

We use the heat conduction equation

$$\frac{\partial T}{\partial t} - \chi \Delta T = \frac{c\gamma |E|^2 (1 - R)}{2\pi c_v} \exp(-\gamma z), \quad (3.10)$$

where R is the optical reflection coefficient (we assume normal incidence of the laser radiation). The solution of Eq. (3.10) at $z = 0$ for $\tau_p \gg \chi^{-1}\gamma^{-2}$ has the form

$$\Delta T = \frac{c|E|^2 (1 - R)}{\pi} \left(\frac{\tau_p}{\pi \kappa c_v}\right)^{1/2}, \quad (3.11)$$

where $\kappa = \chi c_v$ is the thermal conductivity.

(2) The density of nonequilibrium carriers.

Let us write down the equation for the density of the nonequilibrium carriers taking into account the rate of laser generation, linear and Auger recombinations and the diffusion

$$\frac{\partial}{\partial t} n_e(z) + \frac{n_e(z)}{\tau} + \gamma_A n_e^3(z) - D_e \Delta n_e(z) = \sigma E^2 \exp(-\gamma z) \quad (3.12)$$

[2] The case for which G_d depends on n_d is considered in Sec. 5.3.3.

with the boundary condition

$$\left.\frac{\partial n_e(z)}{\partial z}\right|_{z=0} = 0, \qquad (3.13)$$

where $\sigma = (1-R)\gamma c/(2\pi\hbar\omega)$.

Consider the quasistationary regime, for which $\gamma^2 D_e, \gamma_A n_e^2 > \tau_p^{-1}$ and use in Eq. (3.12) the approximation

$$\gamma_A n_e^3(z,t) \cong \gamma_A n_e^2 n_e(z), \qquad (3.14)$$

where $n_e = n_e(z)|_{z=0}$ is the density of the nonequilibrium carriers on the surface.

Then, from Eq. (3.12) we have the equation

$$(\gamma_A n_e^2 - D_e\Delta + \tau^{-1})\, n_e(z) = \sigma|E|^2 \exp(-\gamma z). \qquad (3.15)$$

The solution of this equation at $z=0$ with the boundary condition (3.13) has the form

$$n_e = \left[\frac{\sigma|E|^2}{(\gamma_A n_e^2 + \tau_s^{-1})^{1/2}}\right]\left[(\gamma_A n_e^2 + \tau_s^{-1})^{1/2} + D_e^{1/2}\gamma\right]^{-1}, \qquad (3.16)$$

where τ_s is the time of the linear surface recombination.

Now let us consider various limiting cases of the formula of interest in practice (3.16).

In the case of rapid surface linear recombination ($\tau_s^{-1} > \gamma_A n_e^2, D_e\gamma^2$) from Eq. (3.16) we obtain

$$n_e = \frac{\sigma|E|^2\tau_s}{1+\gamma(D\tau_s)^{1/2}}. \qquad (3.17)$$

In the case of rapid diffusion and rapid Auger recombination ($\tau_s^{-1} < \gamma_A n_e^2 < D_e\gamma^2$) it follows from Eq. (3.16) that

$$n_e = \frac{\sigma^{1/2}|E|}{(\gamma_A\gamma^2 D_e)^{1/4}}. \qquad (3.18)$$

Finally, in the case of rapid Auger recombination and slow diffusion $\gamma_A n_e^2 > \tau_s^{-1}, \gamma D_e$ we have from Eq. (3.16)

$$n_e = \frac{\sigma^{1/3}|E|^{2/3}}{\gamma_A^{1/3}}. \qquad (3.19)$$

In the following we will study the case (3.17), which was realized in experiments of Refs. [63, 73]. Then, substituting Eqs. (3.17) and (3.11) into Eq. (3.9) and using the expression thus obtained for ξ in Eq. (3.7), we represent the latter in a form convenient for comparison with the experiment

$$\ln(n_d) = \ln(\text{const}) + \frac{-\dfrac{E_{A0}^0 - E_{ee}^0}{kT_0} + \dfrac{C_2 W}{T_0}}{1 + \dfrac{C_1 W}{T_0}}, \qquad (3.20)$$

where $W = \tau_p c|E|^2/2\pi$ is the energy density of the laser pulse,

$$C_1 = \frac{2(1-R)}{(\pi\kappa c_v\tau_p)^{1/2}}, \qquad (3.21)$$

$$C_2 = \frac{|\theta_A|(1-R)}{\rho c_l^2 k}\left[\frac{2k\alpha}{(\pi\kappa c_v\tau_p)^{1/2}} + \theta_g\left(\frac{\tau}{\tau_p^2 D}\right)^{1/2}\frac{1}{\hbar\omega}\right]. \qquad (3.22)$$

Let us make numerical estimates of the constants of the present EDT theory – C_1 and C_2 for Ge with the help of Eqs. (3.21) and (3.22). We use the following values of the parameters: $\omega = 2.7\times10^{15}\ s^{-1}$, $\tau_p = 20$ ns, $\theta_g = -10$ eV, $T_0 = 300$ K, $\rho = 5.3\ g\cdot cm^{-3}$, $c_l = 5\times10^5\ cm\cdot s^{-1}$, $R = 0.36$, $\beta = 5.7\times10^{-6}\ degree^{-1}$, $\kappa = 0.6\ W\cdot m^{-1}\cdot degree^{-1}$, $|\theta_A| \cong 10$ eV. For laser intensities I_L used in experiments of Ref. [63] ($10^6\ W\cdot cm^{-2} \le I_L \le 5\times10^6\ W\cdot cm^{-2}$), the time of the surface recombination is $\tau_s = \tau = 10^{-8}$ s [23]. Then, from Eq. (3.18) we have $C_1 = 4.8\ degree\cdot cm^2\cdot mJ^{-1}$ and from Eq. (3.16) $C_2 = 3.4\ degree\cdot cm^2\cdot mJ^{-1}$ and $C_2/T_0 = 1.1\times10^{-2}\ cm^2\cdot mJ^{-1}$. As we will see in Sec. 3.3, these numerical estimates satisfactorily correspond to the experimental values.

We formulate now the basic conclusions which follow from the EDT model of the laser defect formation considered here.

(1) For $W < W_m$ the laser-induced defects arise in a vicinity of the initial centers. Consequently, concentration of the laser generated defects is proportional to the density of initial defects $n_d(t=0)$ (in Eq. (3.20) (const) ~ $n_d(t=0)$).

(2) The process of the defect formation under PLI has a quenching character. The number of defects under the conditions of validity of Eq. (3.17) grows with increasing W according to the law (3.20), which is determined by the parameters of the present EDT theory: $E_{A0}^0 - E_{ee}$, C_1 (Eq. (3.21)), and C_2 (Eq. (3.22)).

(3) The dependence of n_d on the amplitude of the laser field can have a character different from Eq. (3.20) in the case of validity of the condition (3.18) or (3.19).

(4) Under the condition

$$(E_{A0}^0 - E_{ee}^0 - \theta_A\xi) < 0 \qquad (3.23)$$

the defects arise nonthermally (without thermal activation).

3.3. Comparison with Experimental Results [63][3]

First of all we consider the data for Ge in the case of irradiation by nanosecond pulses from a ruby laser.

The surface recombination rate S was deduced from measurements of steady state photoconductivity. At each value of the laser pulse energy density W the dependence of S on the number of pulses N was obtained. After $N = 10$ - 20 pulses S reached stationary value S_{st}. Then the differences $\Delta S = S_{st} - S_0$ were plotted versus W. The value of S is proportional to the concentration of laser-induced surface recombination centers.

In Fig. 8 curves in $\Delta S(W)$ for two samples with the lifetimes $\tau_1 = 20$ μs and $\tau_2 = 100$ μs are represented (curves 1 and 2, respectively). Solid lines in Fig. 8 were calculated from Eq. (3.20) with the following parameters: $E^0_{A0} - E^0_{ee} = 0.17$ eV, $C_2 = 8.5$ degree·cm^2·mJ^{-1} (sample τ_1), $(E^0_{A0} - E^0_{ee}) = 0.17$ eV, $C_2 = 15$ degree·cm^2·mJ^{-1} (sample τ_2). The magnitude of C_1 was taken equal to 4 degree·cm^2·mJ^{-1} in accordance with Ref. [58]. From Fig. 8 one can clearly see rather good agreement between experimental points and the dependencies calculated from Eq. (3.20).

The energy of bulk defect formation in Ge under the thermal action (quenching) is about 2.0 eV for vacancies [60]. This value is much greater than the parameters of $E^0_{A0} - E^0_{ee}$ obtained in Ref. [63]. Such a large decrease of the defect formation energy shows the important role of electronic excitation.

The experimentally measured value of the parameter C_2 is of the same magnitude as that obtained below from Eq. (3.22). Elimination of the surface deformation term in the expression (3.22) ($|\theta_A| = 0$) causes a large deviation of the theoretical curve from the experimental points. This is clearly seen from comparison of the solid line 1 and the dashed line calculated in accordance with Eq. (3.20) at $E^0_{A0} - E^0_{ee} = 0.17$ eV, $C_1 = 4$ degree·cm^2·mJ^{-1} and $C_2 = 0$.

The marked difference of effectiveness of laser-induced defect creation for samples with different initial defect density (samples τ_1 and τ_2) is in agreement with the EDT model suggested in this work. When the initial defectiveness of a semiconductor is increased, the energy required for a new center formation becomes lower. In our case the value of $E^0_{A0} - E^0_{ee}$ diminished from 0.17 eV for the sample τ_2 to 0.1 eV for the sample τ_1. The suggestion about the important role of the initial defects is supported by the data on laser-induced defect localization obtained in Ref. [54]. It was found that the defects are distributed in the surface layer with a thickness of 40 - 60 nm. This value is much less than the absorption depth of the Nd : YAG laser radiation (10^3 nm) used in Ref. [63] and the heat diffusion length (1 - 2×10^3 nm).

[3] The experimental results were obtained by P.K. Kashkarov.

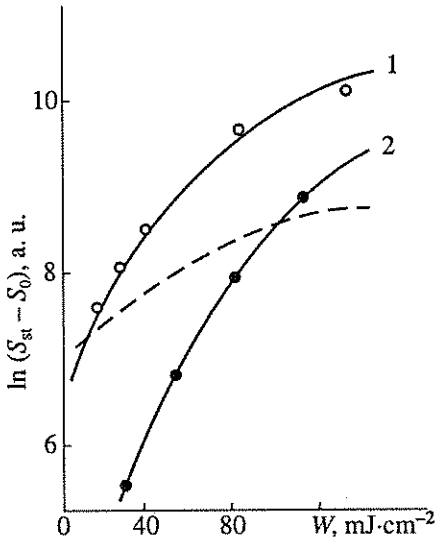

Fig. 8. *Laser-induced change of the surface recombination velocity in Ge versus laser pulse energy density W. Initial lifetimes are $\tau_1 = 20$ μs (1) and $\tau_2 = 100$ μs (2). Solid lines are calculated in accordance with Eq. (3.20). Dashed line is calculated for sample τ_1 neglecting deformation in Eq. (3.20) [63].*

Application of photoluminescence (PL) for registration of defects in III - V materials makes it possible to carry out experiments at room and liquid nitrogen temperatures. In the latter case the temperature of the crystal did not increase between the PLI and PL-measurements.

Let us consider the data for GaAs obtained in the case of ruby laser irradiation. The most intense was the band edge line with the maximum at $\hbar\omega = 1.5$ eV ($T = 80$ K). The dependencies of the PL intensity I and the PL signal U on the number of laser pulses N was obtained for each value of W. The magnitudes of I and U reached their steady state values I_{st} and U_{st} after the action of 4 - 10 laser pulses. PLI caused the decrease of PL and PC, the relative change of PL and PC being rather close to each other. This shows that the effects observed are due to the generation of nonradiative recombination centers. In this case, concentration of the centers induced by PLI follows the relation:

$$n_d \sim (I^{-1} - I_0^{-1}),$$

where I_0 is the initial PL intensity.

In Fig. 9 the dependencies of $\ln [I_{st}^{-1}(W) - I_0^{-1}]$ are shown for two temperatures of PLI 300 and 80 K. It is seen from Fig. 9 that the efficiency of defect formation decreases at lower temperature ($T = 80$ K). Therefore, the thermal activation plays a definite role in defect generation, and for GaAs the following relation is valid:

$$E^0_{A0} - E^0_{ee} - \theta_A \xi > 0.$$

The comparison of the experimental data with the expression (3.20) allowed one to estimate the parameters $E^0_{A0} - E^0_{ee} = 0.18$ eV and $C_2 = 22$ degree·cm^2·mJ^{-1}.

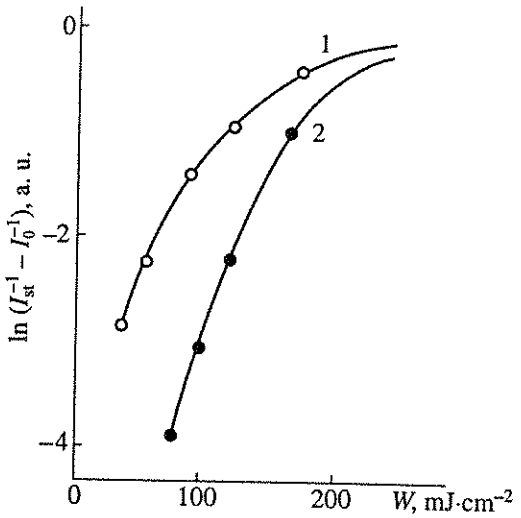

Fig. 9. *Laser-induced change of luminescence of GaAs sample. Laser irradiation and photoluminescence measurements were carried out at temperature 300 K (1) and at 80 K (2) [63].*

As in the case of germanium, the magnitude of $E_{A0}^0 - E_{ee}^0$ obtained is much less than the known energy of thermal defect formation 0.7 - 2.0 eV [60].

Thus the studies of the defect formation in Ge and GaAs under subthreshold pulse laser irradiation ($W < W_m$) show that the experimental results obtained are in reasonable agreement with the conclusions of the EDT model proposed here. The comparison of measured data with calculated dependencies enabled us to estimate the effective defect formation energy in our experiments: $E_{A0}^0 - E_{ee}^0 = 0.1$ - 0.2 eV. This value is much less than the formation energy of thermodefects $E_{A0}^0 = 1.5$ - 2.5 eV, which is evidence of the important role of local electronic excitation in the defect generation under PLI.

As we have pointed out already, aside from Eq. (3.20), the dependencies n_d on W under different conditions can be described by relations of either (3.18) or (3.19) type. The dependence in the form of Eq. (3.18), i.e., $n_d \sim \exp\left[\dfrac{E_d^0 - C|E|}{kT_0}\right]$ was in fact observed in CdS crystals [65].

In follows from the EDT model that the efficiency of laser induced defect generation is different for surfaces with (111) and (100) crystallographic orientation because of the difference of elastic and thermal parameters for these surfaces.

If the laser defect formation is considered from the viewpoint of the EDT model the possibility of laser induced EDT instabilities on a semiconductor surface (Sec. 2) should be taken into account. The latter should enhance the role of long-range deformations in this mechanism and lead to the appearance of ordered defect structures. Let us proceed to consideration of this problem.

3.4. Formation of Surface Cell Periodic Structures Due to DTI in GaP

When studying pulsed laser-induced surface defect formation in Secs. 3.1 - 3.3, we assumed that the generated defects are distributed uniformly along the surface over the irradiated spot. In Ref. [71] formation of periodic (with period 7 - 8 μm) defect structures on the surface of GaP was recorded under irradiation by UV pulses of the excimer laser. Note that radiation of the excimer laser is characterized by highly homogeneous intensity distribution over the beam cross-section.

The surface (111) of n-GaP monocrystals ($n_e = 10^{17}$ cm^{-3}) etched in the mixture of HNO_3 and HCl (1 : 1) was irradiated by the excimer laser pulses ($\tau_p = 20$ ns, $\lambda = 308$ nm) with energy density varied within an interval of $W = 50$ - 760 mJ·cm^{-2} at normal incidence. The defects were studied using a J-SM-U3 raster electron microscope.

After laser irradiation with $W > 10^2$ mJ·cm^{-2} the appearance of periodic dark spots was recorded on the surface (Fig. 10). The mean distance between the spots was 7 - 8 μm and did not change when W increased up to the melting threshold $W \approx 300$ mJ·cm^{-2} (cf. Fig. 10). In doing so, the mean size of the spots increased with increasing W.

The darkening of the local spots on the surface in the secondary electron emission regime occurs due to the increase of electronic work function. Earlier an increase of the surface potential of GaP under similar laser irradiation was observed, connected with the defect generation [72]. Based on these observations, one may assume that the dark spots observed in REM appear also due to laser-induced defects.

The periodicity in the defect distribution indicates the development of certain surface instability. Let us show that the observed picture can be explained within the framework of the DTI theory developed in Sec. 2.

It follows from the results of Sec. 2.3.3 that the coupled deformation-temperature grating appears on the surface due to the development of DTI

$$\xi = \xi_q \exp(iqx + \lambda t) + \text{c. c.},$$
$$T = T_q \exp(iqx + \lambda t) + \text{c. c.} \qquad (3.24)$$

The DTI occurs when the growth rate of DTI $\lambda > 0$ (λ is given by Eq. (2.33b)). For GaP at $K = 10^{12}$ erg·cm^{-3}, $\alpha = 5 \times 10^{-6}$ degree^{-1}, $\rho = 9$ g·cm^{-3}, $c_l = 3 \times 10^5$ cm·s^{-1}, $\theta = 10$ eV we have in Eq. (2.33b)

$$\theta K\alpha / \rho c_e^2 \sim 10^{-4} \ll |\partial E_g / \partial T| \sim 6 \times 10^{-4} \text{ eV·degree}^{-1}.$$

Thus in Eq. (2.22) one has $\varepsilon_{TT} \gg R_T$ (we put $R_n = 0$). The critical intensity of the DTI is found from Eq. (2.33b):

$$I_{cr} = \frac{cE_{cr}^2}{2\pi} = q\frac{\chi\gamma\varepsilon'' \hbar c_v c}{4\omega(\partial\varepsilon''/\partial\omega)}\left|\frac{\partial E_g}{\partial T}\right|^{-1} \lesssim 10^7 \text{ W·cm}^{-2}. \qquad (3.25)$$

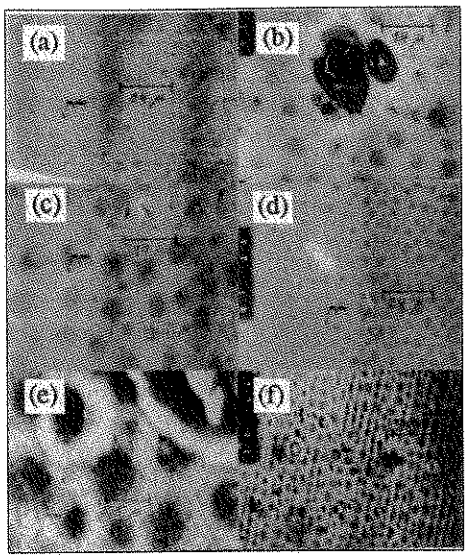

Fig. 10. *Raster electron microscope photograph of GaP surface: before laser irradiation (a), after irradiation with 0.1 (b), 0.16 (c), 0.26 (d), 0.48 (e), 0.76 J·cm^{-2} (f).*

The value of q determines the period of the grating, which under conditions considered is given by Eq. (2.31b):

$$d = 2\pi (4\tau_p \chi)^{1/2} \sim 8\ \mu\text{m}. \qquad (3.26)$$

Thus the period is independent of pump intensity. Note that this result is valid only in the limit $\varepsilon_{TT} \gg R_T$, and in the opposite limit we have $\varepsilon_{TT} \ll R_T$, $d \sim E^{-2}$.

The direction of q is determined by the direction of the crystallographic axis. There are three equivalent axes on the (111) surface. In this case the DTI development must lead to the appearance of three gratings with the rulings perpendicular to the axes. The intersection of these three gratings forms the cell structure of the deformation and temperature field distribution on the surface.

The spatially periodic deformation-temperature field (3.23) leads to formation of the periodic surface defect structure. In fact, in a general case, when no assumptions are made about a particular form (3.6) of the generation rate G_d, one can write

$$G_d = G_d(T, \xi) = G_{d0} + \frac{\partial G_d}{\partial T} T_1 + \frac{\partial G_d}{\partial \xi} \xi_1. \qquad (3.27)$$

If the defects arise nonthermally in the case for which the condition (3.23) holds, then in Eq. (3.27) $\partial G_d / \partial T_1 = 0$, and from Eqs. (3.26) and (3.23) we have

$$G_d = G_{d0} + \frac{\partial G_d}{\partial \xi} \xi_d \exp(iqx + \lambda t). \qquad (3.28)$$

In the case of thermal fluctuation generation rate, from Eqs. (3.23) and (3.7), assuming $\Delta T = T_1$ and expanding Eq. (3.7) in a power series of T_1 and ξ, one obtains

$$n_d = \text{const}\left(1 + \frac{2(E^0_{A0} - E^0_{ee})\,\theta_A \xi_q}{kT_0^2 |\partial E_g / \partial T|} \cos qx e^{\lambda t}\right). \qquad (3.29)$$

When deriving Eq. (3.29) we have used the condition

$$(E^0_{A0} - E^0_{ee}) / T_0 |\partial E_g / \partial T| \gg 1$$

and the relation

$$T_1 = -\xi_1 \varepsilon_{TT} \theta / (\chi\gamma\delta_T - \varepsilon_{TT}) |\partial E_g / \partial T|,$$

which follows from Eqs. (2.37a, b) at $\varepsilon_{TT} \gg \chi\gamma\delta_T$.

As is seen from Eq. (3.28) or (3.29), both for thermal and nonthermal defect generation the periodic defect grating is formed on the surface due to the development of DTI. On a (111) surface the intersection of three such defect gratings forms the defect cell structure. The time of grating formation t_0 is determined by Eqs. (2.30) and (2.26) ($\tau_{j0}^{-1} = 0$, $\varepsilon_{TT} \gg R_T$):

$$t_0^{-1} \equiv \lambda^{-1} = \chi [(\varepsilon_{TT} / \gamma\chi)^2 - q^2] \sim 10^9\ \text{s}^{-1} > \tau_p^{-1}, \qquad (3.30)$$

at $\chi \sim 0.2$ cm^2·s^{-1}.

Thus the results on critical intensity (Eq. (3.25)), the period of structure (Eq. (3.26)) and the time of grating development (Eq. (3.30)), obtained using the DTI theory of Sec. 3.3.3 correspond to the experimental results of Ref. [71] (Fig. 10).

It follows from the experimental results of Ref. [73] that the defect generation mechanism in GaP seems to be nonthermal (i.e., in GaP inequality (3.23) holds). Thus, the cell structure formation on the GaP surface is likely to occur due to the deformation modulation of the generation rate (Eq. (3.28)).

In this section we have considered the mechanism of defect grating formation due to the GDI. In principle, the mechanism of the electron DDI can also lead to a similar picture (see Sec. 4.3.4). To identify the relevant mechanism of cell structure formation in GaP, further experimental studies are necessary. One, for example, can irradiate GaP surface with pulses of different duration and use the fact that the GDI grating period $d \sim \sqrt{\tau_p}$, whereas the DDI period is independent of τ_p (see Sec. 4.3.4).

4. FORMATION OF PERIODIC DEFECT-DEFORMATIONAL STRUCTURES ON SURFACES AND IN FILMS

As it was shown in Sec. 3, laser irradiation greatly enhances the rate of point defect production in semiconductors. A similar situation takes place in metals, where the laser-produced heating and deformation lead to the enhanced rate of point defect (vacancy) generation.

The simplest kinetic equation governing vacancy production under laser irradiation of a metal surface can be written as [16]

$$\frac{\partial n_v}{\partial t} = [n_{v0}(T) - n_v]/\tau_v \equiv G_v - R_v, \qquad (4.1)$$

where n_{v0} is the equilibrium vacancy concentration taking into account laser-induced rise of temperature T and medium strain,

$$n_{v0}(T) = n\exp\left[\frac{(-E_{v0}) - \theta_v\xi}{kT}\right].$$

Here $n = a^{-3}$ is the concentration of atoms, $\theta_v = -Ka^3$, G_v and R_v are generation and recombination rates, correspondingly, τ_v is the defect lifetime

$$\tau_v = l_v^2/D_v, \qquad (4.2)$$

l_v is the mean distance between the defects' sink, and D_v is the diffusion coefficient.

At highly elevated temperatures, chemical reactions on the surface, which is in contact with a chemically active environment, may dominate in the process of laser-induced pumping of vacancies into the subsurface layer. As estimated in Ref. [16], the powerful fluxes of vacancies from the surface into the bulk occur in laser-induced high temperature ($T \sim 10^3$ K) oxidation of a metal surface in air ($j_v \sim 10^{21}$ cm^{-2}·s^{-1}), which exceeds the fluxes due to the thermal fluctuating generation of vacancies (10^{17} - 10^{19} cm^{-2}·s^{-1}) by several orders of magnitude. This means that in these conditions the rate of chemical production of vacancies greatly exceeds the thermal-fluctuation rate given by Eq. (4.1). Because the chemical reaction (oxidation) is also a thermal activation process, the rate of chemically produced vacancies on the surface is given by an equation similar to Eq. (4.1)

$$G_v = g\exp[-((E_0 - \theta_0 \operatorname{div} \mathbf{U})/kT), \qquad (4.3)$$

where E_0 is the activation energy of the reaction, θ_0 is the deformation potential of the reaction and g is the rate constant.

Thus, both generation rates – the one due to the thermal fluctuation mechanism (4.1) and the chemical one (4.3) – are modulated by the medium strain. Because point defects, being rigid inclusions into an elastic continuum, deform the latter [30, 31], there appears feedback leading to instabilities of point defect generation and formation of ordered structures of defect concentration during the generation process itself.

In this section we consider two examples of these vacancy generation-deformational instabilities (GDI) – the first one takes place on a metal surface (Sec. 4.1) and the second one – in a metal film (Sec. 4.2).

The periodic defect structures can be formed also in the process of self-consistent deformationally induced redistribution of laser generated defects along the surface. We consider an example of such diffusion-deformational instability (DDI) on a surface of a semiconductor in Sec. 4.3.

As it was mentioned in Sec. 1, the strain wells periodic along the surface are formed as a result of either GDI or DDI development, which are filled with defects, the diffusion of the latter being strongly deformationally suppressed. Due to this circumstance the defects' structure persists for a long time, i.e., a metastable state is formed (see Sec. 4.3.4). Identification of the particular mechanism (GD or DD) responsible for the formation of a given structure can be done on the basis of analysis of the corresponding experimental data (see below).

4.1. Vacancy Generation-Deformational Instability (GDI) on a Surface of a Semi-Infinite Metal

4.1.1. Experimental Observation of Radial Structures on the Surface of Ti

The formation of permanent "star"-like (Fig. 2a) surface structures was observed in experiments of Ref. [74], using Ti polished plates BT1-0 of thickness 7 and 1 mm, irradiated in air by Nd : YAG laser pulses ($\lambda = 1.06$ μm, $\tau_p = 1$ ms) with Gaussian intensity distribution with maximum intensity $I_0 < 10^6$ W·cm^{-2}. Nonpolarized radiation impinged on the surface at normal incidence.

Under irradiation in a vacuum the structures were not formed. A typical radius r_{irr} of the irradiated zone was 2 - 3 mm. At low intensities, formation of an irregular relief was observed (Fig. 11a). With the increase of I_0 up to the critical value $I_{cr} = 6 \times 10^5$ W·cm^{-2} the periodic rays emanating from the centre of the irradiated spot were recorded (Fig. 11b). The number of rays m increased with the distance from the centre of the spot r (Fig. 11c), and at $r = 2.5$ mm amounted to $\sim 10^3$ ($2\pi r/m \sim 10$ μm). The increase of the number of the rays with the increase of r occurred as bifurcation of each ray into two rays (Figs. 11b, 11c, 11d). At a constant value of the irradiated zone radius (r_{irr} = const) the number of rays increased with increasing I_0. Further increase of intensity was accompanied by melting of the center of the spot and formation of rays at the periphery of the spot (Fig. 11d). In some cases at the periphery of the spot the number of rays essentially increased with $2\pi r/m \approx 1$ μm (Fig. 11c). The surface relief had modulated ray-like structure with typical depth (the distance between valleys and peaks) of about 0.5 - 2 μm, as measured with the help of an interference microscope. For the recorded picture of the surface the presence of the ray-like void structure, spatially synchronized with ray-like relief structure, was characterized by the typical void size $\lesssim 2$ μm (Fig. 11e), which essentially enhanced the diffusive component of the reflected light. Similar ray-like relief was recorded also on zirconium.

4.1.2. Theory of the Vacancy GDI

Let us show that the essential features of the experimentally observed picture can be explained from the viewpoint of the vacancy GDI theory [29, 74].

We consider a semi-infinite solid bounded by the surface $z = 0$ upon which the laser light is incident, with Gaussian intensity distribution

$$I = I_0 \exp\left(-\frac{r^2}{r_0^2}\right), \tag{4.4}$$

which generates the vacancy field with concentration n_v in the subsurface layer. The origin of forces appearing in the equations for displacement vector $\mathbf{U}$ and the equation for vacancy concentration due to the vacancy subsystem were discussed in Sec. 1. In the particular case of vacancies, from Eq. (1.1) we have (compare with Eq. (2.4)):

$$\frac{\partial^2 \mathbf{U}}{\partial t^2} = c_t^2 \Delta \mathbf{U} + (c_l^2 - c_t^2)\,\text{grad div}\,\mathbf{U} - \frac{\theta_v}{\rho}\,\text{grad}\,n_v. \tag{4.5}$$

Based on the fact that the "star"-structures were not found under irradiation in a vacuum, we assume the oxidation mechanism of vacancy generation and postulate using Eq. (4.3) the following equation for vacancy concentration

$$\frac{\partial n_v}{\partial t} = D_v \Delta n_v - \frac{n_v}{\tau_v} + \frac{\theta_v n_v D_v}{kT}\Delta\,\text{div}\,\mathbf{U} + g\exp\left[-\frac{E_0 - \theta_0\,\text{div}\,\mathbf{U}}{kT}\right] \tag{4.6}$$

with the boundary conditions

$$\left.\frac{\partial n_v}{\partial z}\right|_{z=0} = 0, \quad n_v|_\infty = 0. \tag{4.6a}$$

Eqs. (4.5) and (4.6), together with corresponding boundary conditions (4.16), (4.17), and (4.6a) constitute the closed system of equations for description of the vacancy GDI.

If the laser pulse duration is τ_p then the distribution of temperature is given by Ref. [66]

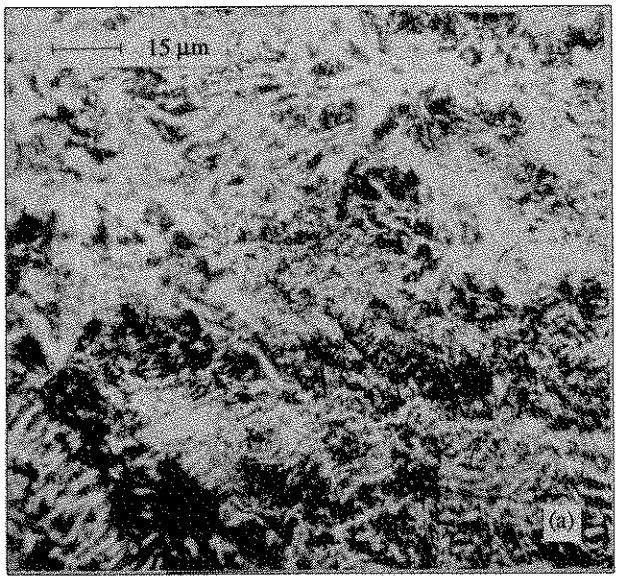

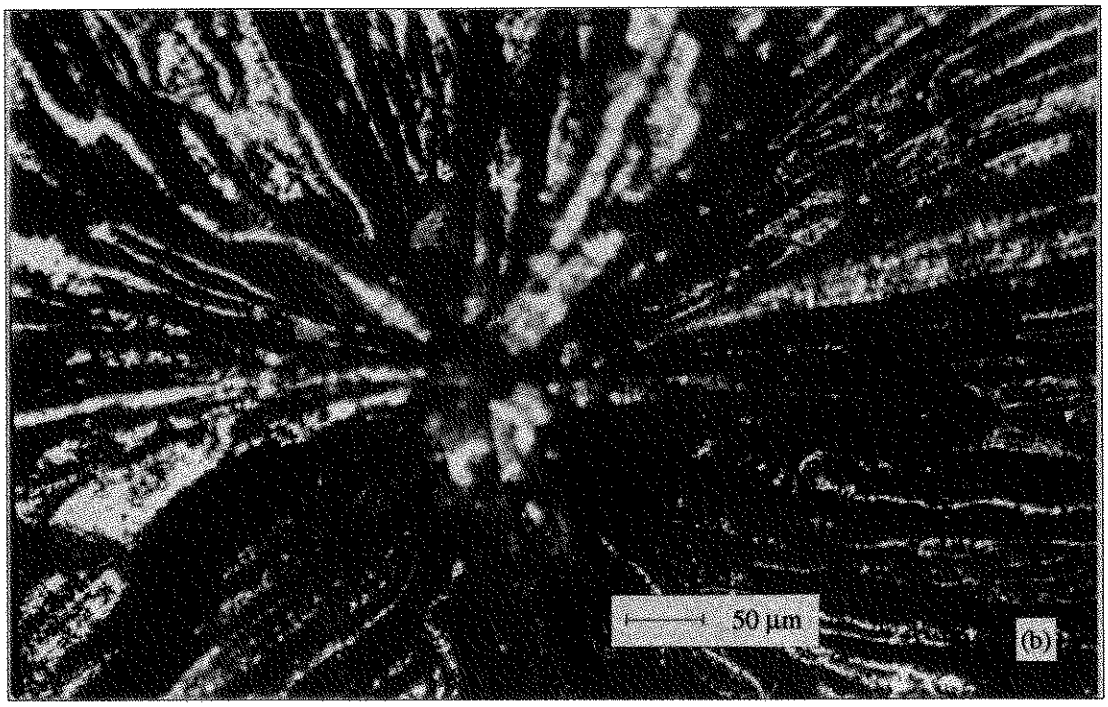

Fig. 11. *Dark-field optical microphotographs of relief formation zones on Ti surface after the action of the laser pulse. Arrows show the direction to the center of the irradiated spot: the formation of irregular relief, $I_0 < I_{cr} = 6 \times 10^5$ W·cm^{-2} (a); ray star relief structure formation in the center of irradiation zone $I_0 \geq I_{cr}$ (b).*

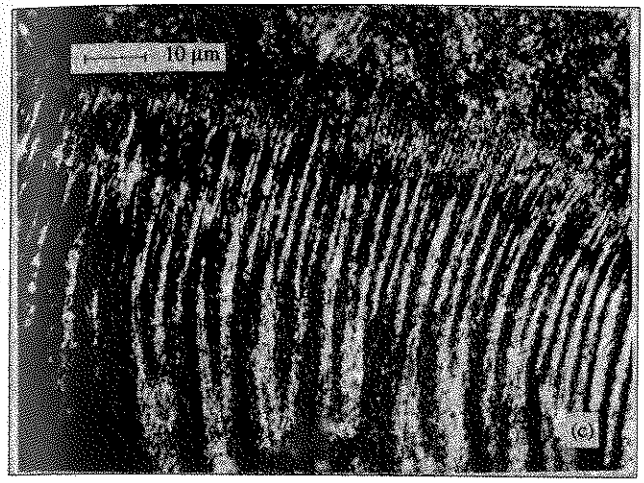

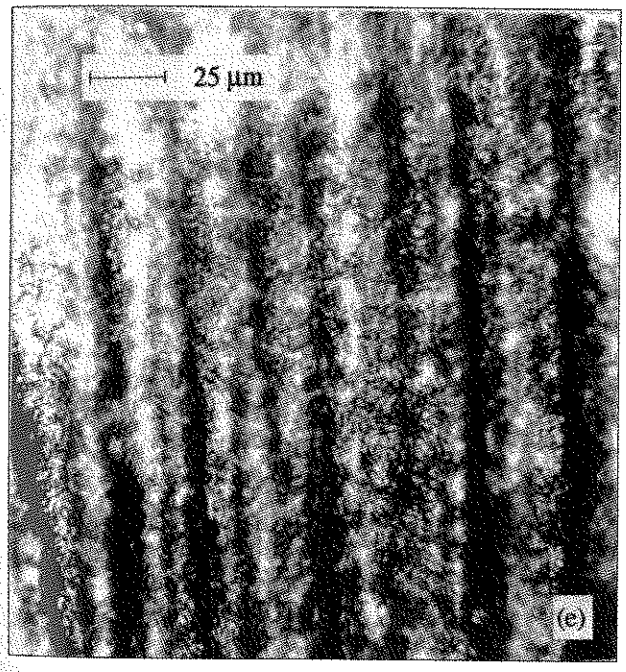

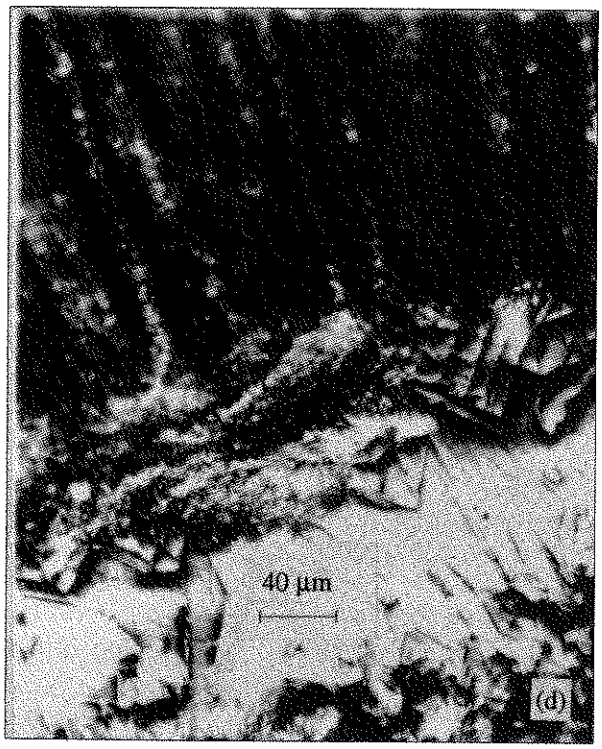

Fig. 11 (contd.). *Dark-field optical microphotographs of relief formation zones on Ti surface after the action of the laser pulse. Arrows show the direction to the center of the irradiated spot: the increase of the number of rays by bifurcation with increase in the distance from the center of the irradiated spot (c); melting of the center of the spot and the shift of the rays to spot periphery, $I_0 \cong 2I_{cr}$ (d); periodic void structure formation (e).*

$$T(r,z,t) = \frac{I_0(1-R)\,r_0^2}{4\chi c_v}\int_0^\infty J_0(\xi r)\exp(-r_0^2\xi^2/4)$$
$$\times\left[e^{-\xi z}\left(1-\Phi\left(\frac{z}{2\sqrt{\chi t}}-\sqrt{\chi t}\xi\right)\right)\right. \qquad (4.7)$$
$$\left.-e^{\xi z}\left(1-\Phi\left(\frac{z}{2\sqrt{\chi t}}+\sqrt{\chi t}\xi\right)\right)\right]d\xi,$$

where $J_0(\xi r)$ is the zero-order Bessel function of the first kind, $\Phi(x)$ is the error integral. Under the condition $\tau_p > r_0^2\chi^{-1}$ the stationary temperature distribution is installed, which in the region $r, z \ll r_0$ has the form

$$T(r,z) = T_0(1 - r^2/2r_0^2 - 2z/\sqrt{\pi}r_0),$$
$$T_0 = \frac{I_0(1-R)\,r_0\sqrt{\pi}}{2\sqrt{2}\chi c_v}. \qquad (4.8)$$

In the opposite limit $\tau_p < r_0^2\chi^{-1}$ under the condition for $z \ll 2\sqrt{\chi t}$ one obtains the following expression

$$T(r,z,t) = T_0\exp(-r^2/r_0^2)\,(1 - z\sqrt{\pi/\chi t}/2),$$
$$T_0 = \frac{I_0(1-R)\sqrt{\chi t}}{\sqrt{\pi}\chi c_v}. \qquad (4.9)$$

Taking into account Eqs. (4.8) and (4.9), the generation rate under the conditions $\theta_0 \operatorname{div} \mathbf{U} \ll kT_0$, $r < r_0$ can be represented in the form

$$g\exp\left(-\frac{E_0 - \theta_0 \operatorname{div}\mathbf{U}}{kT}\right)$$
$$\approx g_0\exp\left(-\gamma z - \frac{r^2}{r_{\text{eff}}^2}\right)\left(1 + \frac{\theta \operatorname{div}\mathbf{U}}{kT_0}\right), \qquad (4.10)$$

where (under the condition $\tau_p > r_0\chi^{-1}$) the value of T_0 is determined by Eq. (4.8) and γ, r_{eff} is given by

$$\gamma = \sqrt{\pi}E_0/(kT_0\sqrt{\chi t}),\quad r_{\text{eff}} = (kT_0/E_0)^{1/2}r_0. \qquad (4.11)$$

Under the condition $\tau_p < r_0\chi^{-1}$ the value of T_0 is determined by Eq. (4.9) and γ, r_{eff} is given by

$$\gamma = 2E_0/(kT_0r_0\sqrt{\pi}),\quad r_{eff} = (2kT_0/E_v)^{1/2}r_0. \quad (4.12)$$

We represent the variables in the form $n_v = n_0 + n_1$, $\mathbf{U} = \mathbf{U}_0 + \mathbf{U}_1$, where n_0, $\mathbf{U}_0$ are monotonous (along the surface) solutions and n_1, $\mathbf{U}_1$ are spatially nonmonotonous additions. Taking into account Eq. (4.10), from Eq. (4.6), neglecting vacancy drift in the following equation for n_1, we obtain

$$\frac{\partial n_1}{\partial t} = D_v\Delta n_1 - \frac{n_1}{\tau_v} + g_0\exp(-\gamma z - r^2/r_0^2)\,(\theta_0/kT_0)\,\mathrm{div}\,\mathbf{U}_1|_{z=0} \quad (4.13)$$

with the boundary conditions (4.6a), where n_v is substituted by n_1. In the right-hand side of Eq. (4.13) we assumed that γ^{-1} is much less than the characteristic length of $\mathrm{div}\,\mathbf{U}_1$ variation.

Let us determine whether the condition drift of vacancies can be neglected. At $\theta_0 \sim \theta_v$ and $g_0 \sim \tau_p^{-1}n_0$ the generation term on the r.h.s. of Eq. (4.13) is greater than the neglected drift term (4.6), if $d > d_0 = 2\pi\sqrt{D_v\tau_p}$, i.e., in the case of generation of sufficiently large scale structures. At $D = 10^{-5}$ cm$^2\cdot$s^{-1}, $\tau_p = 10^{-3}$ s, $d_0 = 6\times10^{-4}$ cm. Thus, we confine ourselves to consideration of large scale structures and neglect the vacancy drift.

We represent vector $\mathbf{U}_1$ as a sum of the longitudinal and the transverse components:

$$\mathbf{U}_1 = \mathbf{U}_{1l} + \mathbf{U}_{1t};\ \mathrm{rot}\,\mathbf{U}_{1l} = 0,\ \mathrm{div}\,\mathbf{U}_{1t} = 0. \quad (4.14)$$

The equation for $\mathbf{U}_1$ follows from Eq. (4.5). Taking into account Eq. (4.14), we have (omitting the subscript 1 further on)

$$\frac{\partial^2\mathbf{U}_\alpha}{\partial t^2} = c_\alpha^2\Delta\mathbf{U}_\alpha - \delta_{\alpha,l}\,\mathrm{grad}\left(\frac{\theta_v n_1}{\rho}\right), \quad (4.15)$$

where $\alpha = l, t$; $\delta_{\alpha,l} = 0$ for $\alpha = t$; $\delta_{\alpha,l} = 1$ for $\alpha = l$.

The boundary conditions for $\mathbf{U}$, corresponding to the axial symmetry of laser beam Eq. (4.4) have the form

$$\frac{\partial U_r}{\partial z} + \frac{\partial U_z}{\partial r} = 0,\quad \frac{1}{r}\frac{\partial U_z}{\partial\varphi} + \frac{\partial U_\varphi}{\partial z} = 0, \quad (4.16)$$

$$\frac{\partial U_z}{\partial z} + \left(1 - 2\frac{c_t^2}{c_l^2}\right)\left(\frac{\partial U_r}{\partial r} + \frac{U_r}{r} + \frac{1}{r}\frac{\partial U_r}{\partial\varphi}\right) - \frac{\theta_v n_1}{\rho c_l^2} = 0. \quad (4.17)$$

Consider first the case of generation of rays and assume the following form for the deformation $\xi = (\mathrm{div}\,\mathbf{U})_{z=0}$ at $z = 0$

$$\xi = A\,(r/r_{eff})^m\cos m\varphi\exp(-r^2/r_{eff}^2 + \lambda t), \quad (4.18)$$

where m is an integer. In the case of stationary temperature distribution, given by Eq. (4.8), A is a constant in Eq. (4.18), λ is the growth rate, independent of time. In the case of nonstationary temperature distribution, given by Eq. (4.9) $A = f_1(t)$ and $\lambda = f_2(t)$ are slow functions of time

$$f_\alpha^{-1}\partial f_\alpha/\partial t \ll \lambda,\quad \alpha = 1, 2.$$

The solutions of Eq. (4.13) under the conditions $r/r_{eff} \ll m$, $\gamma \gg m^{1/2}r_{eff}^{-1}$, $[(\lambda + \tau_v^{-1})/D_v]^{1/2}$ and accounting for the boundary condition (4.6a) have the form

$$n_1 = \varepsilon A\exp(-\delta z - r^2/r_{eff}^2 + \lambda t) \times (r/r_{eff})^m\cos m\varphi/D_v\delta\gamma, \quad (4.19)$$

where $\varepsilon = g_0\theta_0/kT_0$, $\delta = (q^2 + (\lambda + \tau_v^{-1})/D_v)^{1/2}$, $q^2 = 4(m+1)/r_{eff}^2$.

Taking into account the solution for n_1 – Eq. (4.19), we obtain the following expressions for the displacement vector components ($i = r, \varphi, z$):

$$U_i = \frac{r^{m-1}}{r_{eff}^m}\exp(-r^2/r_{eff}^2 + \lambda t)\,\Psi_i \times (a_iMe^{-\kappa_t z} + b_iNe^{-\kappa_l z} + Mc_i\Phi e^{-\delta z}), \quad (4.20)$$

where M, N are constants, $\Psi_r = m\cos m\varphi$, $\Psi_\varphi = -m\sin m\varphi$, $\Psi_z = r\cos m\varphi$; $a_r = a_\varphi = 1$, $a_z = -\kappa_l$, $b_r = b_\varphi = -\kappa_t$, $b_z = q^2$, $c_r = c_\varphi = -\lambda^2$, $c_z = \lambda^2\delta$; $\kappa_{l,t} = (q^2 + \lambda^2/c_{l,t}^2)^{1/2}$, $\Phi = 1 - (R(q^2 - \delta^2)c_l^2/D_v\gamma\delta)/(\lambda^2 + c_l^2(q^2 - \delta^2))$.

The pump parameter R_v is determined by the expression

$$R_v = -g_0\theta_0|\theta_v|/kT_0\rho c_l^2. \quad (4.21)$$

Substituting the solutions (4.20) into the boundary conditions (4.16), (4.17), we obtain the system of two linear equations for N and M. Equating the determinant of this system of equations to zero, we obtain the dispersion equation for the vacancy GDI, governing the dependence of λ on m:

$$(\kappa_t^2 + q^2)^2 - 4q^2\kappa_t\kappa_l = \frac{\lambda^2}{c_l^2}\,\frac{R_v((\kappa_t^2 + q^2)^2 - 4q^2\kappa_t\delta)}{(\lambda^2/c_l^2 + (q^2 - \delta^2))\,D_v\gamma\delta - R_v(q^2 - \delta^2)}. \quad (4.22)$$

This equation is similar to the dispersion equation of EDTI (compare Eq. (4.22) with Eq. (2.22)).

The left-hand side of Eq. (4.22) is the Rayleigh determinant, governing the dispersion law of the surface acoustic waves [76]. The r.h.s. takes into account the generation of vacancies (θ_0) and their interaction with the elastic continuum (θ_v).

Under the condition $\lambda^2/c_{t,l}^2 \ll q^2$, $(\lambda + \tau_v^{-1})/D_v$ from Eq. (4.22) we obtain the dispersion relation